narra j

Original Article

Exploring the potential of *Laportea decumana* extract compounds as COX-1 and COX-2 inhibitors: An in silico study

Eva S. Simaremare[1,2], Fransiska Kurniawan[1], Rika Hartati[1] and Daryono H. Tjahjono[1*]

[1]School of Pharmacy, Institut Teknologi Bandung, Bandung, Indonesia; [2]Department of Pharmacy, Faculty of Mathematics and Natural Sciences, Universitas Cenderawasih, Jayapura, Indonesia

*Corresponding author: daryonohadi@itb.ac.id

Abstract

Laportea decumana (Roxb.) Wedd., known as itchy leaves, is traditionally used for pain relief due to its bioactive compounds. However, previous studies were limited by resource-intensive in vivo methods and a lack of mechanistic insights into cyclooxygenase (COX)-1 and COX-2 binding. The aim of this study was to identify compounds in the n-hexane and ethyl acetate extracts of *L. decumana* with potential as COX-1 and COX-2 inhibitors and to predict their binding affinity and stability within the binding pocket through molecular dynamics simulations. Leaves collected from Arso, Keerom Regency, Papua, Indonesia, were dried, sieved into simplicia, and macerated with n-hexane to obtain a n-hexane extract. The residual simplicia was further macerated with ethyl acetate to produce an ethyl acetate extract. N-hexane extract compounds were analyzed by gas chromatography-mass spectrometry (GC-MS), and ethyl acetate extract compounds by liquid chromatography-mass spectrometry (LC-MS). Identified chemicals were used in in silico evaluations targeting COX-1 and COX-2. This study identified ten compounds with high performance in docking analysis, which were further evaluated by molecular dynamics. The n-hexane extract contained 31 compounds, while the ethyl acetate extract contained 27. Among these, 4,8,12,16-tetramethylheptadecan-4-olide from the n-hexane extract demonstrated the strongest affinity for both COX-1 and COX-2, with binding free energies of -41.62±1.03 kcal/mol and -33.05±0.11 kcal/mol, respectively. Its interactions were comparable to those of native ligands, with superior binding free energy. In the ethyl acetate extract, pseudosantonim demonstrated the highest affinity for COX-1 (-24.41±1.32 kcal/mol), while arteamisinine showed strong potential as a COX-2 inhibitor (-23.53±0.30 kcal/mol). In conclusion, 4,8,12,16-tetramethylheptadecan-4-olide was the most potent COX-1 and COX-2 inhibitor, pseudosantonim was the most effective COX-1 inhibitor, and arteamisinine demonstrated COX-2 inhibitory potential. Further validation through in vitro or in vivo studies is recommended.

Keywords: *Laportea decumana*, analgesics, 4O1Z, 5IKR, cyclooxygenase

Introduction

Laportea decumana (Roxb.) Wedd., commonly referred to as itchy leaves, is a medicinal plant indigenous to Eastern Indonesia, including Nusa Tenggara, Maluku, and Papua [1]. Traditionally, this plant is utilized for pain relief and alleviation of physical exhaustion associated with exertion, postpartum recovery, or trauma [2-4]. The local population acquires the leaves from markets, forests, or home gardens and applies them directly to painful areas such as the back, arms,

Received: October 13, 2024 - Accepted: February 26, 2025 - Published online: March 23, 2025

abdomen, and legs [3]. The plant's trichomes contain acetylcholine and histamine, which adhere to the skin and exert analgesic effects [5]. The release of these bioactive compounds induces vasodilation by expanding blood vessel pores, thereby enhancing blood flow and promoting pain relief [1].

A previous study demonstrated that *L. decumana* leaves contain secondary metabolites, including alkaloids, steroids, terpenes, flavonoids, and phenolics [6]. Additionally, in vivo assessments of various extracts indicated that the highest percentage of pain inhibition and anti-inflammatory activity was observed in the n-hexane extract, followed by the ethyl acetate and ethanol extracts [3]. The interaction of these compounds with analgesic and anti-inflammatory protein was hypothesized to involve cyclooxygenase (COX) inhibition, thereby preventing the conversion of arachidonic acid into pain and inflammatory mediators such as prostaglandins.

COX increases oxygen levels in fatty acids and peroxides and serves as the primary target of nonsteroidal anti-inflammatory drugs (NSAIDs) for inflammation control [7]. COX-1 and COX-2 share similar catalytic mechanisms, both requiring peroxide activation, though COX-1 necessitates a higher concentration [8,9]. Important amino acid residues, including Arg120, Tyr355, Ser530, and Tyr385, regulate the oxygenase site, which is approximately 20% smaller in COX-1 than in COX-2. Additionally, COX-2 possesses a unique hydrophilic side pocket near Phe518, which restricts COX-1 binding [10,11]. COX enzymatically converts arachidonic acid into prostaglandins, with COX-1 facilitating thromboxane A_2 synthesis and COX-2 mediating the production of prostaglandin E_2 and prostacyclin [12]. Although COX-2 is primarily associated with inflammatory responses, COX-1 disruption can impair platelet aggregation [9,13,14]. Historically, COX-1 has been regarded as the predominant pro-inflammatory isoform, given its role in gastrointestinal protection and platelet function regulation [15,16]. The interaction of bioactive compounds from *L. decumana* leaves with analgesic can be investigated through in vitro and in vivo studies, though a validated methodology is required. Computational approaches, particularly molecular docking and molecular dynamics simulations, provide cost-effective predictions of compound interactions with biological targets such as COX-1 and COX-2 [17].

The pharmacological potential of *L. decumana* has been investigated in both traditional and scientific contexts [3]. Ethnobotanical evidence supports its use in alleviating pain, physical exhaustion, postpartum discomfort, and trauma [18]. Previous studies have identified bioactive secondary metabolites, and in vivo evaluations of various extracts have demonstrated analgesic and anti-inflammatory activity [2,6,19]. However, these studies are limited by the resource-intensive nature of in vivo methodologies and the insufficient exploration of mechanisms underlying the selective binding of bioactive compounds to COX-1 and COX-2. Furthermore, computational approaches, such as molecular docking and molecular dynamics simulations, remain underutilized in elucidating these interactions. The aim of this study was to identify compounds in the n-hexane and ethyl acetate extracts of *L. decumana* with potential as COX-1 and COX-2 inhibitors and to predict their binding affinity and stability within the binding pocket through molecular dynamics simulations. By identifying potent and selective inhibitors, this research provides foundational insights for the development of novel analgesic and anti-inflammatory therapies derived from *L. decumana* compounds.

Methods

Study design and setting

This study employed an experimental and in silico computational approach to investigate the pharmacological potential of *L. decumana* leaves as a source of bioactive compounds targeting COX-1 and COX-2. It integrated traditional ethnobotanical practices with advanced extraction, analytical, and in silico techniques to identify active compounds, evaluate molecular interactions with COX enzymes, and assess the potential as selective anti-inflammatory agents. The study was conducted from October 2022 to December 2023. *L. decumana* leaves were collected from Arso, Keerom Regency, Jayapura, Papua, Indonesia, and identified at the Herbal Laboratory of Materia Medica, Batu, Malang Regency, East Java, Indonesia. The study involved collecting and preparing plant materials, identifying chemical compounds, and conducting computational analyses to elucidate molecular interactions.

Tools and materials

The experimental tools included liquid chromatography-mass spectrometry (LC-MS) (UPLC-MS Waters-Class Tandem Xevo G2S QTOF, Waters Corporation, Massachusetts, USA) and gas chromatography-mass spectrometry (GC-MS) (Agilent GC 7890A-MS 5975C, Agilent Technologies, California, USA). The hardware used consisted of an Asus laptop with an Intel Core i3 7th Gen processor (ASUSTeK Computer Inc, Taipei, Taiwan), 2GB RAM, 320GB HDD, Intel VGA GMA Graphics, and Intel HD Graphics. The software utilized included ChemSketch 2021.1.3 (ACD, Toronto, Canada) [20], MGLTools 1.5.6 with AutoDock 4.2 (The Scripps Research Institute, La Jolla, California, USA) [21,22], Amber16 and AmberTools 17 (UCSF, San Francisco, California, USA) [23], UCSF Chimera (UCSF, San Francisco, California, USA) [24], Avogadro 1.95 [25], and Biovia Discovery Studio Visualizer 2019 (19.1.0.219) (Dassault Systèmes BIOVIA, Waltham, Massachusetts, USA) [26].

Sampling and determination of *Laportea decumana* leaves

Samples were collected from Arso, Keerom Regency, Jayapura, Papua, Indonesia, ensuring representation of the local *L. decumana* population. Identification and documentation involved field observations, photographic records, and specimen collection to verify morphological characteristics. Reference materials, including botanical guidebooks and nomenclature lists specific to the *Laportea* genus, were consulted for accurate classification. Taxonomic identification from kingdom (Plantae) to species (*Laportea decumana* (Roxb.) Wedd.) was conducted at the Herbal Laboratory of Materia Medica, Batu, Malang Regency, East Java, Indonesia, to confirm species identity.

Extraction of *Laportea decumana* leaves simplicia

The extraction procedure employed a sequential solvent-based approach to obtain n-hexane and ethyl acetate extracts. Fresh *L. decumana* leaves were collected in 1–5 large sacks (approximately 25 kg, wet weight), cleaned to remove dirt, and rinsed under running water. The leaves were air-dried on newspaper and then oven-dried at 50°C for one week. The dried leaves were ground into a fine powder using a high-speed Philips Blender 3000 Series HR2042/50 (Philips Domestic Appliances, Amsterdam, Netherlands) at approximately 500 rpm and sieved through a 100 µm pore sieve. The resulting simplicia was stored in a dry container for one day prior to extraction. The maceration process involved immersing 2 kg of simplicia in 2.5 L of n-hexane (technical grade) for 3×24 hours. The mixture was then filtered through filter paper (Whatman Grade 4, 20–25 µm) using a glass funnel, yielding 19 g of n-hexane extract with a recovery rate of 0.95%. The residual simplicia underwent further maceration with 2.5 L of ethyl acetate (technical grade) for 3×24 hours. Following filtration and evaporation of the filtrate, 119.6 g of ethyl acetate extract was obtained, representing a recovery rate of 5.1% [27].

Analyzing chemical compounds from the n-hexane extract using gas chromatography-mass spectrometry (GC-MS)

The sample was analyzed using an Agilent GC 7890A-MS 5975C system operated in electron ionization mode. The temperature program commenced at 40°C for 2 minutes, followed by an increase to 70°C at a rate of 5°C/min, with no hold time. Subsequently, the temperature was raised to 280°C at a rate of 20°C/min, again with no hold, and finally increased at 30°C/min to 299°C, where it was held for 3 minutes. The total analysis time was 22.13 minutes. The inlet temperature was set to 250°C with a 5:1 split ratio, a sample injection volume of 1 µL, a flow rate of 4.5 mL/min, a pressure of 5.953 psi, and a transfer line temperature of 280°C. The mass spectrometer was equipped with a DB-5ms column, with an ion source temperature of 230°C, a quadrupole temperature of 150°C, and a detector temperature of 230°C. Data interpretation was performed through sequential steps, including data acquisition, processing, querying, matching, scoring, and ranking. Mass spectrometry (MS) data were utilized for chemical compound identification by analyzing individual peaks based on retention time (RT), quantifying compound abundance, and assessing molecular weight (m/z) along with fragmentation patterns. A reference database was employed to verify molecular identities and determine compound concentrations within the sample. The findings were systematically presented in graphical or tabular formats for further interpretation.

Analyzing chemical compounds from the ethyl acetate extract using liquid chromatography-mass spectrometry (LC-MS)

A qualitative analysis of *L. decumana* leaf extract was conducted to evaluate its suitability for in silico testing using an ultra-performance liquid chromatography-mass spectrometry (UPLC-MS) Waters-Class Tandem Xevo G2S QTOF system. This analysis included the subsequent evaluation of the isolates. A millipore filter (0.54 µm) was used to filter 50 mg of the isolate dissolved in acetonitrile. The liquid chromatography (LC) Quadrupole Time-of-Flight (QTOF) system was coupled with an Electrospray Ionization (ESI) source operating in both positive and negative modes, and 5 µL of sample filtrate was injected [28]. ESI parameters included a capillary temperature of 120°C, an atomizing gas flow rate of 500 L/hour, and a voltage of 3 kV. The system operated within a mass range of *m/z* 100–5,000 at a source temperature of 110°C. Chromatographic separation was achieved using an Acquity HSS C18 column (1.8 µm, 2.1×150 mm) at a flow rate of 0.3 mL/min. The mobile phase consisted of H_2O (solvent A) and acetonitrile (solvent B). The elution profile began with isocratic elution at a ratio of 95:5 (A:B) from 0–1 minute, followed by linear gradient elution of solvent A from 95% to 5% over 1–6 minutes. This process was followed by isocratic elution at 0:100 (A:B) from 6 to 7 minutes, a linear gradient elution of solvent A from 0% to 100% between 7 and 7.5 minutes, and a final isocratic elution at 95:5 (A:B) from 7.5 to 9 minutes. Data analysis was performed using the Personal Compound Database (Agilent Technologies, Santa Clara, USA), which processed LC-MS data to identify compounds based on RT, molecular weight, fragmentation patterns, and compound presence. The results were visualized for further interpretation [29].

Molecular docking

Protein preparation

Protein molecules and native ligands for COX-1 and COX-2 enzymes were prepared for analysis. The proteins were obtained from the Protein Data Bank (PDB) (https://www.rcsb.org/) using PDB IDs 4O1Z for COX-1 and 5IKR for COX-2. Structural modifications were performed to simplify the docking system, including the removal of water molecules, cofactors, and other non-essential components. Protein structures were constructed using Avogadro 1.95 [31,32]. The ten compounds with the highest scores, based on their rank, interactions with key COX amino acid residues, and binding affinity, underwent further evaluation through molecular dynamics simulations.

Ligand preparation

A total of 31 compounds were identified from the n-hexane extract and 27 from the ethyl acetate extract, all of which were evaluated as potential ligands. Each test compound was initially drawn using ChemSketch 2021.1.3 [20], followed by three-dimensional (3D) structural modeling and geometry optimization using Avogadro 1.95 (https://avogadro.cc/). The Universal Force Field (UFF) was applied to ensure molecular stability and physiological relevance [25,31].

Docking parameters

Docking parameter validation was performed by redocking meloxicam to COX-1 and mefenamic acid to COX-2 using AutoDock 4.2 and MGLTools 1.5.6 (Scripps Research Institute, La Jolla, California, USA) [21,32]. The docking protocol involved validating the method through redocking experiments, with meloxicam for COX-1 and mefenamic acid for COX-2. The docking results were considered valid when the root mean square deviation (RMSD) value between the docked pose and the crystallographic pose was ≤2 Å [33]. The calculations utilized the Lamarckian Genetic Algorithm (GADock) method [21]. The grid box size was set to 40×40×40 points with a grid spacing of 0.375, centered on the binding sites of COX-1 and COX-2. Using Genetic Algorithm-Local Search (GA-LS) searches, 100 docking runs were conducted, following the default protocol for other parameters [21,32,33]. Validation was carried out using RMSD as the parameter, which measured atomic positional differences between experimental and docked or predicted structures. An RMSD value below 2.0 Å was generally regarded as acceptable for confirming the docking method's accuracy [33]. Lower RMSD values indicated a closer alignment of the predicted ligand pose with the native conformation, thereby reflecting greater prediction accuracy. Docking clustering was performed to categorize ligand conformations based on their

positional and orientational proximity to the native ligand within the protein's active site. This approach facilitated the identification of the most optimal and representative ligand conformations for interaction with the target COX.

Binding site definition

The binding sites for docking were defined based on the positions of co-crystallized ligands in the PDB structures (4O1Z for COX-1 and 5IKR for COX-2). This approach facilitated accurate targeting of the active site regions, which were known to interact with NSAIDs [34]. Blind docking was not conducted, as the binding sites had been thoroughly characterized.

Binding mode analysis

The docking results were visualized using BIOVIA Discovery Studio Visualizer 2019 (19.1.0.219) to identify key interactions, such as hydrogen bonds, π-π stacking, and hydrophobic interaction [26]. The validity of the docking parameters was assessed through the RMSD value. Ligand interactions with amino acid residues were analyzed to evaluate binding affinities and potential inhibitory activity. Additionally, molecular docking results were further assessed by calculating the binding free energy (ΔG) of the ligand compounds in comparison to the native ligand and their interactions with COX-1 and COX-2 amino acid residues [33].

Molecular dynamics simulation

Molecular dynamics simulations were conducted to assess the stability of ligand-protein interactions over time [38-40]. The parameters analyzed included binding pose, binding free energy, and RMSD. Amber16 software was used to simulate molecular behavior, with preparation files generated using the Parmchk module (UCSF, San Francisco, California, USA). Molecular dynamics simulations were performed for 200 ns using the General Amber Force Field (GAFF) (UCSF, San Francisco, California, USA) for ligand parameterization and Amber FF14SB for proteins. Sodium ions (Na^+) were incorporated to neutralize the complex, ensuring overall charge balance. The transferable intermolecular potential with 3 points (TIP3P) water model was applied, with a box edge set 10 Å from the solute. Simulations were maintained under constant pressure and temperature conditions at 310 K. Energy minimization was performed using 5000 steps of the steepest descent method in the Particle Mesh Ewald Molecular Dynamics (PMEMD) module of Amber16. Following gradual heating to 310 K, all constraints were incrementally removed until equilibrium was reached. Trajectories were recorded every 10 ps throughout the 200 ns simulation to analyze atomistic interactions. A 200 ns simulation duration was selected to balance computational efficiency, system stability, and biological relevance, ensuring adequate representation of binding interactions and free energy calculations. Bond interactions and RMSD were analyzed using the CPPTRAJ module of Amber17 (UCSF, San Francisco, California, USA). The binding free energy of each complex was determined using the molecular dynamics trajectories and the mmpbsa.py module [38]. A total of 500 snapshots were extracted from the final 10 ns of the 200 ns simulation for binding energy calculations. For ligand-COX-1 and ligand-COX-2 complexes, Molecular Mechanics Poisson-Boltzmann Surface Area (MMPBSA) calculations were performed with an internal dielectric constant of 4.0 [39]. Ligand-enzyme interactions were assessed through complex visualization using BIOVIA Discovery Studio Visualizer 2019 (19.1.0.219), with important amino acid residues identified as Arg120, Ser530, Tyr355, and Tyr385. Additional residues involved in ligand binding included His90, Ile345, Val349, Leu352, Ser353, Trp385, Phe518, Met522, Ile523 (COX-1), Val523 (COX-2), Gly526, Ala527, Leu531, Leu535, and Leu537 [30,34,40].

Analysis of the optimal ligand candidates for COX-1 and COX-2 inhibition

The selection of the most potent compounds as COX-1 and COX-2 inhibitors was based on binding affinity and stability within the binding pocket during a 200 ns molecular dynamics simulation. Among the ligands from the n-hexane extract and the ethyl acetate extract subjected to molecular docking, the ten highest-ranking compounds were advanced to the MD simulation phase. The selection criteria included interactions with key COX amino acid residues—Arg120, Tyr355, Tyr385, and Ser530—which are essential for inhibiting prostaglandin synthesis [30]. Additionally, hydrophobic interactions play a crucial role in determining the optimal conformation of the ligand within the COX active site, specifically involving residues such as

Val116, Leu352, Ile345, Ser353, Trp385, Val349, Phe518, Met522, Ile523/Val523, Gly526, Ala529, and Leu531 [40]. A higher number of interactions with these residues was predicted to enhance inhibitory potency. The total number of these interactions was referred to as TR.

Additionally, the screening process incorporated binding free energy analysis, where a more negative ΔG value indicated a stronger inhibitory effect on COX. From the top ten MD simulation results, the three ligands demonstrating the highest binding affinity and structural stability, as determined by RMSD analysis, were selected. The best-performing ligands from the n-hexane and ethyl acetate extracts were then compared with the native ligand based on binding position and energy. Stability against COX-1 and COX-2 was assessed at 0 ns, 50 ns, 100 ns, 150 ns, and 200 ns. Based on trajectory analysis, one compound was recommended as the most promising COX-1 and COX-2 inhibitor.

Results

Analysis of *L. decumana* leaf extract by mass spectroscopy

Qualitative analysis of *L. decumana* leaf extract using mass spectrometry identified terpene secondary metabolites as the predominant components (**Table 1** and **Table 2**). The n-hexane extract contained 31 compounds, primarily diterpenes, monoterpenes, sesquiterpenes, terpenoids, and essential oils. The sesquiterpene hexahydro farnesyl acetone was the most abundant compound, comprising 42.14% of the total, followed by 4-(1,1,3,3-tetramethylbutyl)-phenol at 6.44% (**Table 1**). The terpenoid group, including monoterpenes and diterpenes, accounted for approximately 18.04% of the total compounds, with key constituents such as phytol, γ-cadinene, and 2,6-dimethyl-2,6-octadiene. Although the proportion was lower than that of sesquiterpenes, terpenoids contributed to the extract's bioactivity diversity. Phenolic compounds were also present, comprising approximately 6.86% of the total, with notable constituents including 4-(1,1,3,3-tetramethylbutyl)-phenol and 2,4-bis(1,1-dimethylethyl)-phenol. Essential oils accounted for 3.36% of the composition, including apiol and O-methyl-chavicol, along with minor components such as esters, carotenoids, and other volatile compounds (**Table 1**).

Table 1. Chemical compounds identified in the n-hexane extract of *Laportea decumana* using gas chromatography-mass spectrometry (GC-MS)

Code	Compound name	m/z	RT (min)	%	Type of compound
H1	Hexahydrofarnesyl acetone	268	23.77	42.14	Sesquiterpenes [41]
H2	4-(1,1,3,3-tetramethylbutyl)-phenol	206	21.63	6.44	Phenolic [42]
H3	Methyl 3-(3,5-di-tert-butyl-4-hydroxyphenyl) propionate	292	24.86	6.42	Phenolic [43]
H4	Phytol	296	23.65	5.54	Geranylgeraniol [44]
H5	Farnesyl acetone	262	24.63	5.30	Sesquiterpenes [45]
H6	(E, E, E)-3,7,11,15-tetramethyl-, acetate, 2,6,10,14-Hexadecatetraen-1-ol	332	29.50	4.68	Diterpenes [46]
H7	4,8,12,16-tetramethylheptadecan-4-olide	324	29.28	4.07	Terpenoid [47,48]
H8	γ-cadinene	204	17.07	2.35	Sesquiterpenoids [49]
H9	2,6-dimethyl-2,6-octadiene	138	9.09	2.31	Terpenoid [50,51]
H10	Dihydro-actinidiolide	180	17.59	1.96	Karatenoid [52,53]
H11	Trans-geranylacetone	194	15.34	1.91	Monoterpenes [54]
H12	(E, E)- 6,10-dimethyl-5,9-dodecadien-2-one	208	5.78	1.89	Curcumin [55]
H13	2,5,5,8a-tetramethyl-4-methylene-6,7,8,8a-tetrahydro-4H,5H-chromen-4a-yl hydroperoxide	238	20.70	1.81	Terpenoid [56]
H14	2-isopropenyl-5-methylhex-4-enal	152	9.44	1.70	Monoterpenoids [60-62]
H15	2-ethylhexyl ester 2-propenoic acid	184	11.70	1.68	Esther [60]
H16	3-methyl-2-(3,7,11-trimethyl dodecyl) furan	292	24.49	1.56	Terpenoid [61]
H17	8-oxo-2-nonenal	154	11.44	1.17	Lipid [62]
H18	6-methyl-5-hepten-2-one	126	7.96	0.88	Diterpenes [63]
H19	Apiol	222	19.88	0.88	Essential oil [64]
H20	D-limonene	136	8.74	0.87	Monoterpenes [65]
H21	O-methyl-chavicol	148	12.72	0.87	Essential oil [66]

Code	Compound name	m/z	RT (min)	%	Type of compound
H22	5-isopropenyl-2-methyl-7-oxabicyclo[4,1,0]heptan-2-ol	168	12.91	0.71	Essential oil [67]
H23	5,5-dimethyl-4-(3-methyl-1,3-butadienyl)-1-oxaspiro[2,5]octane	206	17.22	0.45	Essential oil [68]
H24	3-4-(2,6,6-trimethyl-2-cyclohexen-1-yl)-buten-2-one	192	14.90	0.45	Diterpenes [69]
H25	Caryophyllene	204	14.96	0.45	Sesquiterpenes [70]
H26	Cedrene	204	14.10	0.45	Sesquiterpenes [71]
H27	2,4-bis(1,1-dimethyl ethyl)-phenol	206	16.72	0.42	Phenol [72]
H28	1,7-dimethyl-naphthalene	156	15.05	0.28	Volatile oil [73]
H29	2-acetoxy-1,1,10-trimethyl-6,9-epidioxydecalin	268	16.19	0.14	Monoterpenes [74]
H30	β-ionone	192	16.12	0.13	Cyclic diterpenes [75]
H31	2,6-di-tert-butyl-p-benzoquinone	220	15.71	0.09	Monocyclic monoterpenoids [72]

RT: retention time; m/z: mass-to-charge ratio, where z represents the number of ion charges

The 27 chemical compounds identified from the ethyl acetate extract were classified into terpenes, flavonoids, alkaloids, saponins, and glycosides (**Table 2**). The predominant compounds by proportion included dihydroactinidiolide (27.16%) (a coumarin derivative), digiprolactone (17.90%) (a glycoside), platycogenic acid B (6.43%) (a saponin), and fawcettiine (6.16%) (an alkaloid). The extract demonstrated considerable chemical diversity, with flavonoids accounting for 30.45% of the total, including nobiletin (3.95%), apigenol (3.49%), and robustaflavone (0.15%). Saponins represented 11.42%, with platycogenic acid B (6.43%) and tenuifolin (2.10%) as the principal components. Sesquiterpenes constituted 6.28%, while steroids and triterpenoids comprised 6.35%, with neogogenin acetate (1.62%) and 12β-hydroxycimigenol (1.30%) as the major constituents (**Table 2**).

Table 2. Chemical compounds identified in the ethyl acetate extract of *Laportea decumana* using liquid chromatography-mass spectrometry (LC-MS)

Code	Compound name	m/z	RT (min)	%	Type of compound
E1	Dihydroactinidiolide	180.24	14.77	27.16	Coumarin [76]
E2	Digiprolactone	196.24	8.45	17.90	Glycoside [77]
E3	Platycogenic acid B	534.68	14.80	6.43	Saponin [78]
E4	Fawcettiine	351.40	13.36	6.16	Alkaloid [79]
E5	Arteamisinine	206.13	12.20	5.86	Sesquiterpenes lactone [80]
E6	Fibraurin	372.40	16.63	5.41	Diterpenoid [81]
E7	Terminolic acid	504.69	14.87	4.38	Pentacyclic triterpenoid glucoside [82]
E8	11-O-p-coumarylnepeticin	616.91	17.33	3.97	Flavonoid [83]
E9	Nobiletin	402.39	16.58	3.95	Flavonoid [84]
E10	Platycogenic acid A	534.68	14.45	3.87	Saponin [78]
E11	Apigenol	270.24	14.34	3.49	Flavonoid [85]
E12	1α,2α,3β,19α,23-pentadroxyurs-12-en-28-oic acid-28-O-β-D-xylopyranoside	620.81	16.63	3.22	Triterpenoid [86]
E13	Tenuifolin	680.82	14.67	2.10	Saponin [87]
E14	Neogogenin acetate	458.67	17.38	1.62	Steroid [88]
E15	12β-hydroxycimigenol	504.70	15.55	1.30	Triterpene-glycoside [89]
E16	Melazolide A	212.24	5.93	0.78	Terpenoid [90]
E17	Kirenol	338.50	14.56	0.74	Diterpenoid [91]
E18	1,1,6-trymethyl-1,2-dihydronaphthalene	172.27	12.01	0.36	Tetraterpenoid [92]
E19	Pseudosantonim	264.32	10.59	0.27	Flavonoid
E20	Oxypyllenodiol A	238.32	14.15	0.25	Steroid [93]
E21	Anemonin	192.17	7.90	0.15	Terpenoid [94]
E22	Robustaflavone	538.46	16.71	0.15	Flavonoid [95]
E23	Dihydroxyeudesm-11(13)-en-12-oic acid	236.35	12.60	0.14	Sesquiterpenes [96,97]
E24	Kaempferol	286.23	12.66	0.13	Flavonoid
E25	Genistin	432.38	10.24	0.09	Flavonoid [98,99]
E26	Izalpinin	284.26	16.56	0.07	Flavonoid [100]
E27	Pterodontoside F	270.35	11.03	0.05	Sesquiterpenes [101]

RT: retention time; m/z: mass-to-charge ratio, where z represents the number of ion charges

Validation of docking parameters for ligand-protein interactions in COX-1 and COX-2 enzymes

The redocking process successfully restored the ligand conformation, closely aligning with the respective crystal structure and yielding an RMSD value of less than 2 Å, thereby validating the docking parameters employed (**Figure 1**). Hydrogen bonds were observed at Ser530, while hydrophobic interactions were identified at Val349, Ala527, and Leu352 in the meloxicam-COX-1 and mefenamic acid-COX-2 complexes, respectively (**Figure 2**).

The amino acid composition of COX-1 and COX-2 enzymes was largely similar, with the primary distinction at position 523, where isoleucine in COX-1 creates steric hindrance, whereas valine in COX-2 forms a hydrophobic pocket (**Figure 2**). Important amino acid residues involved in COX-ligand interactions included Arg120, which facilitated substrate binding; Ser530, which catalyzed prostaglandin formation; Tyr355, which interacted with NADH cofactors; and Tyr385, which contributed to inhibitor binding. Additional key residues included His90, Ile345, Val349, Leu352, Ser353, Trp385, Phe518, Met522, Ile523 (COX-1), Val523 (COX-2), Gly526, Ala527, Leu531, Leu535, and Leu537 [102,103].

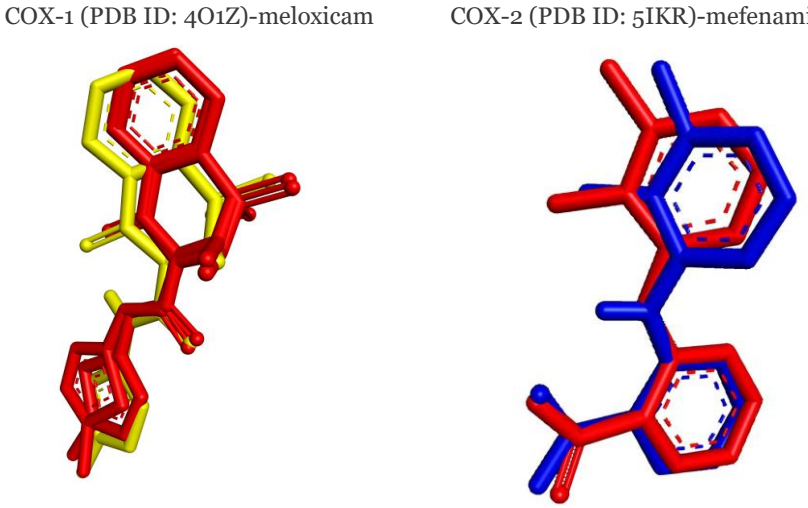

Figure 1. Superimposition of meloxicam and mefenamic acid in cyclooxygenase-1 (COX-1) and cyclooxygenase-2 (COX-2), respectively, before and after redocking with root mean square deviation (RMSD) ≤2 Å, demonstrated minimal deviation between the docked and crystallographic poses, thereby confirming the accuracy of the docking protocol.

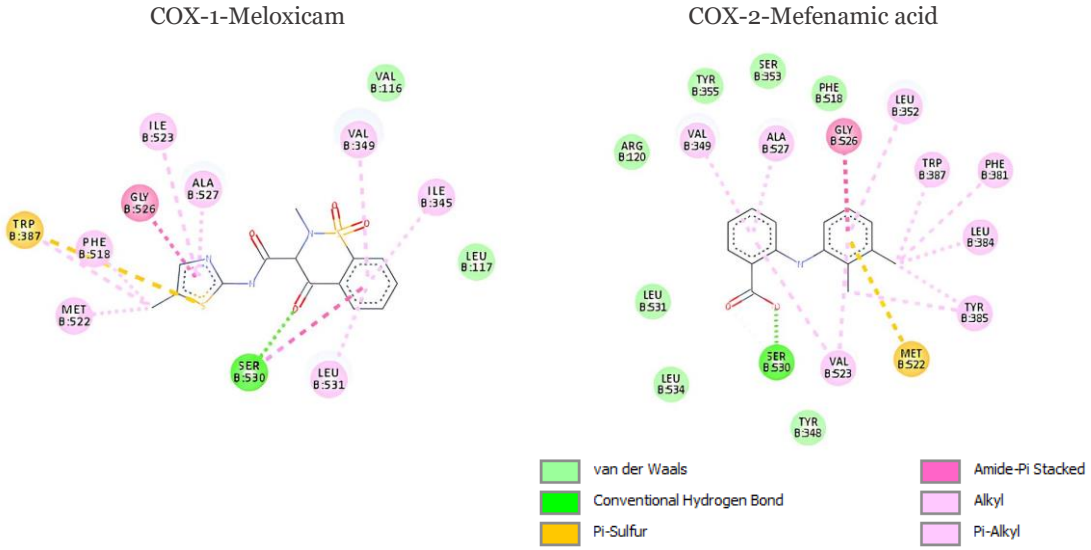

Figure 2. Two-dimensional (2D) interaction map illustrating the binding interactions between native ligands (meloxicam for cyclooxygenase-1 (COX-1) and mefenamic acid for cyclooxygenase-2 (COX-2)) and the important amino acid residues of the protein, highlighting hydrogen bonding, hydrophobic interactions, and other critical interactions between the ligands and amino acid residues.

Molecular docking analysis of ligands from the n-hexane and ethyl acetate extracts with COX-1 and COX-2 receptors

Meloxicam's interaction with COX-1 in molecular docking and dynamics simulations showed alkyl bonds between its thiazole group and Ile345, Ile523, Leu531, Ala527, Phe518, Met522, and Val349. Its carboxamide carbonyl (C=O) formed hydrogen bonds with Ser530, while the amide (NH) bonded with Gly526, and π sulphur with Trp387. The benzene group showed an amide–π interaction with Met522. In COX-2, mefenamic acid's phenyl hydrogen formed hydrogen bonds with Ser530, an alkyl bond with Val346, while its benzoic acid hydrogen formed a π bond with Val349, Ala527, Leu352, Trp387, Phe381, Leu384, Tyr385, Val523. However, the amide (NH) bonded with Gly526, and π sulphur with Trp387.

The clustering results of molecular docking for n-hexane extract ligands against COX-1 and COX-2 are presented in **Figure 3**. The top ten ligands [(E, E, E)-3,7,11,15-tetramethyl-acetate-2,6,10,14-hexadecatetraen-1-ol; 4,8,12,16-tetramethylheptadecan-4-olide; farnesyl acetone; phytol**;** hexahydrofarnesyl acetone; 2,5,5,8a-tetramethyl-4-methylene-6,7,8,8a-tetrahydro-4H,5H-chromen-4a-yl-hydroperoxide; β-ionone; methyl 3-(3,5-di-tert-butyl-4-hydroxyphenyl) propionate; (E, E)- 6,10-dimethyl-5,9-dodecadien-2-one; and 2-acetoxy-1,1,10-trimethyl-6,9-epidioxydecalin] docked with COX-1 (**Figure 3A**) formed at least one hydrogen bond with Ser530 or Arg120. These ligands demonstrated binding poses similar to the natural ligand within the COX-1 binding pocket. The ten ligands (8-oxo-2-nonenal; apiol; dihydro-actinidiolide; 2,4-bis(1,1-dimethyl ethyl)-phenol; 2-ethylhexyl ester 2-propenoic acid; 2-isopropenyl-5-methylhex-4-enal; 3-4-(2,6,6-trimethyl-2-cyclohexen-1-yl)-buten-2-one, 1,7-dimethyl-naphthalene; 5-isopropenyl-2-methyl-7-oxabicyclo[4,1,0] heptan-2-ol; and trans-geranylacetone) in the second cluster formed hydrogen bonds with Ser530; however, their binding free energy values were relatively more positive than those in the first cluster (**Figure 3B**). Eleven additional ligands (o-methyl-chavicol; 1,7-dimethyl-naphthalene; 2,6-dimethyl-2,6-octadiene; 2,6-di-tert-butyl-p-benzoquinone; 3-methyl-2-(3,7,11-trimethyl dodecyl)furan; 5,5-dimethyl-4-(3-methyl-1,3-butadienyl)-1-oxaspiro[2,5]octane; caryophyllene; d-limonene; cedrene; and γ-cadinene) that did not establish hydrogen bonds with the four key residues, showing more positive binding free energy compared to those in the first and second clusters (**Figure 3C**).

Similarly, for docking results of COX-2 (**Figure 3D-Figure 3F**), the top ten ligands (4,8,12,16-tetramethylheptadecan-4-olide;((E, E, E))-3,7,11,15-tetramethyl-acetate-2,6,10,14-hexadecatetraen-1-ol; farnesyl acetone; phytol; β-Ionone; methyl 3-(3,5-di-tert-butyl-4-hydroxyphenyl) propionate; (E, E)- 6,10-dimethyl-5,9-dodecadien-2-one; 2-acetoxy-1,1,10-trimethyl-6,9-epidioxydecalin; 3-4-(2,6,6-trimethyl-2-cyclohexen-1-yl)-buten-2-one; and 4-(1,1,3,3-tetramethylbutyl)-phenol) formed at least one hydrogen bond with Ser530, Tyr385, or Arg120 (**Figure 3D**). The next eight ligands (2,4-bis(1,1-dimethylethyl)-phenol; *trans*-geranylacetone; 2-ethylhexyl ester 2-propenoic acid; apiol; 2-isopropenyl-5-methylhex-4-enal; 5-isopropenyl-2-methyl-7-oxabicyclo [4.1.0] heptan-2-ol; 8-oxo-2-nonenal; and 6-methyl-5-hepten-2-one) displayed binding poses comparable to the native ligand in the COX-2 binding pocket (**Figure 3E**). In contrast, 13 ligands (3-methyl-2-(3,7,11-trimethyldodecyl)furan; hexahydrofarnesyl acetone; γ-cadinene; 2,5,5,8a-tetramethyl-4-methylene-6,7,8,8a-tetrahydro-4H,5H-chromen-4a-yl hydroperoxide; caryophyllene; 2,6-di-*tert*-butyl-*p*-benzoquinone; 1,7-dimethylnaphthalene; dihydroactinidiolide; 2,6-dimethyl-2,6-octadiene; *d*-limonene; and *o*-methyl-chavicol) failed to form hydrogen bonds with key residues and demonstrated more positive binding free energy compared to the native ligand or ligands in other clusters (**Figure 3F**).

The binding affinity of various ligands was analyzed in comparison to the native ligands of COX-1 and COX-2 (**Table 3**). The native ligand for COX-1, meloxicam, had a ΔG of -9.50 kcal/mol, while the native ligand for COX-2, mefenamic acid, had a ΔG of -7.08 kcal/mol. Most ligands showed more negative ΔG values (indicating higher binding affinity) than mefenamic acid in COX-2; however, only one surpassed the affinity of meloxicam in COX-1. Among the tested ligands, 4,8,12,16-tetramethyl-heptadecan-4-olide had the highest binding affinity, with a ΔG of -9.74 kcal/mol for COX-1 and –9.62 kcal/mol for COX-2, exceeding the affinities of both meloxicam and mefenamic acid. Similarly, (E, E, E)-3,7,11,15-tetramethyl-acetate,2,6,10,14-hexadecatetraen-1-ol) showed strong binding to both COX-1 and COX-2, with ΔG values of –9.14

kcal/mol and -9.38 kcal/mol, respectively. In contrast, ligands such as 6-methyl-5-hepten-2-one and o-methyl-chavicol had significantly weaker binding to COX-1 and COX-2, with *ΔG* values of -5.33 kcal/mol and -5.18 kcal/mol, respectively. Overall, these findings suggest that certain non-native ligands possess greater binding affinity than native ligands, highlighting their potential for further development as anti-inflammatory candidates with similar pharmacological properties.

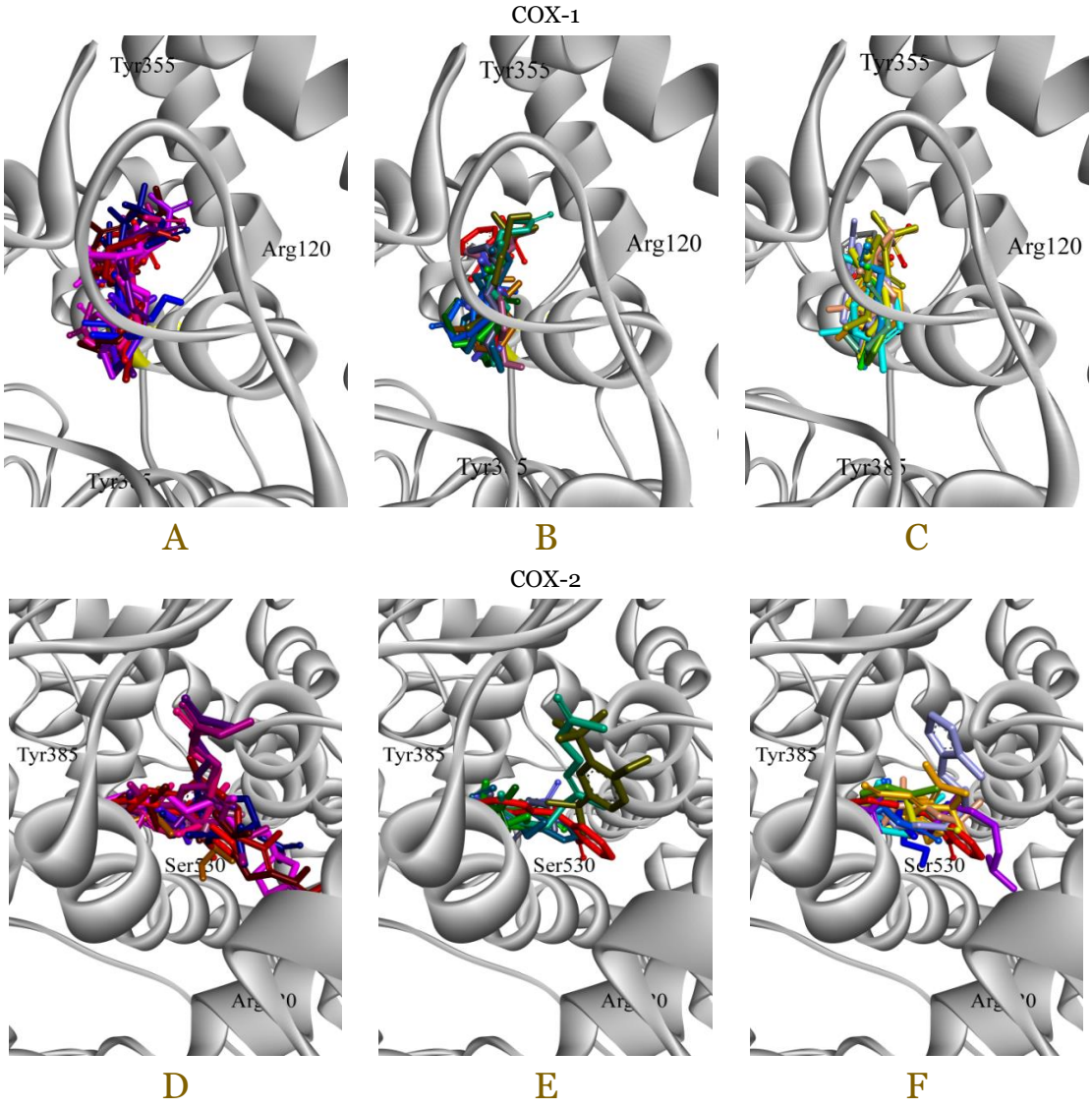

Note:

H1: Lilac	H9: Light moss green	H17: Dark moss	H25: Tan
H2: Dark rose	H10: Bright blue	H18: Light cyan	H26: Cyan
H3: Red purple	H11: Sea foam green	H19: Turquoise	H27: Olive green
H4: Red Hot pink	H12: Dark orchid	H20: Green	H28: Basil green
H5: Hot pink	H13: Caribbean blue	H21: Sky blue	H29: Navy
H6: Maroon	H14: Lilac blue	H22: Forest green	H30: Purple
H7: Pink	H15: Stone blue	H23: Marie gold	H31: Gold
H8: Yellow	H16: Light lavender	H24: Siena burnt	Native ligand: Red

Figure 3. Clustering distribution of docking results from the n-hexane ligand against cyclooxygenase-1 (COX-1) (A-C) and cyclooxygenase-2 (COX-2) (D-F) based on the binding pose of amino acid residues.

Table 3. Characteristics of the binding interactions of ligands from the n-hexane extract with cyclooxygenase-1 (COX-1) and cyclooxygenase-2 (COX-2) based on molecular docking analysis

Code	Ligand	ΔG (Kcal/mol)	
		COX-1	COX-2
Native ligand	Meloxicam	-9.50	
Native ligand	Mefenamic acid		-7.08

Code	Ligand	ΔG (Kcal/mol)	
		COX-1	COX-2
H6	4,8,12,16-tetramethylheptadecan-4-olide	-9.74	-9.62
H7	(E, E, E)-3,7,11,15-tetramethyl-, acetate, 2,6,10,14-hexadecatetraen-1-ol	-9.14	-9.38
H16	3-methyl-2-(3,7,11-trimethyldodecyl) furan	-8.87	-9.28
H5	Farnesyl acetone	-8.47	-8.70
H4	Phytol	-8.40	-8.57
H1	Hexahydrofarnesyl acetone	-7.95	-7.93
H8	γ-cadinene	-7.89	-7.78
H13	2,5,5,8a-tetramethyl-4-methylene-6,7,8,8a-tetrahydro-4H,5H-chromen-4a-yl hydroperoxide	-7.55	-7.01
H25	Caryophyllene	-7.33	-7.12
H26	Cedrene	-7.32	-7.62
H30	β-ionone	-7.15	-7.64
H3	Methyl 3-(3,5-di-tert-butyl-4-hydroxyphenyl) propionate	-7.14	-7.76
H31	2,6-di-tert-butyl-p-benzoquinone	-7.10	-7.40
H12	(E, E)-6,10-dimethyl-5,9-dodecadien-2-one	-7.06	-7.46
H29	2-acetoxy-1,1,10-trimethyl-6,9-epidioxydecalin	-7.02	-6.48
H24	3-4-(2,6,6-trimethyl-2-cyclohexen-1-yl)-buten-2-one	-7.01	-6.98
H28	1,7-dimethyl-naphthalene	-6.96	-6.80
H2	4-(1,1,3,3-tetramethylbutyl)-phenol	-6.87	-6.68
H27	2,4-bis(1,1-dimethylethyl)-phenol	-6.70	-6.56
H11	Trans-geranylacetone	-6.59	-6.94
H23	5,5-dimethyl-4-(3-methyl-1,3-butadienyl)-1-oxaspiro [2.5] octane	-6.58	-6.72
H10	Dihydro-actinidiolide	-6.32	-6.34
H15	2-ethylhexyl ester 2-propenoic acid	-5.84	-6.05
H19	Apiol	-5.71	-6.04
H9	2,6-dimethyl-2,6-octadiene	-5.68	-5.65
H14	2-isopropenyl-5-methylhex-4-enal	-5.58	-5.35
H22	5-isopropenyl-2-methyl-7-oxabicyclo [4.1.0] heptan-2-ol	-5.54	-5.63
H17	8-oxo-2-nonenal	-5.52	-5.40
H20	D-limonene	-5.51	-5.41
H18	6-methyl-5-hepten-2-one	-5.33	-4.92
H21	O-methyl-chavicol	-5.18	-5.29

Δ*G:* binding free energy

The clustering outcomes of docking for the ethyl acetate extract ligands with COX-1 and COX-2 are presented in **Figure 4**. The ten highest-ranking ligands (11-O-p-coumarylnepeticin, nobiletin, fibraurin, dihydroxyeudesm-11(13)-en-12-oic acid, arteamisinine, genistin, oxypyllenodiol, apigenol, kaempferol, and kirenol) from the docking analysis with COX-1 formed at least one hydrogen bond with Ser530 or Arg120 (**Figure 4A**). These ligands demonstrated binding conformations similar to the native ligand occupying the COX-1 binding site. The ten ligands (dihydroxyeudesm-11 (13)-en-12-oic acid; kaempferol; digiprolactone; melazolide; anemonin; kirenol; fawcettiine; robustaflavone; terminolic acid; and 11-o-p- coumarylnepeticin) in the second cluster formed hydrogen bonds with Ser530 (**Figure 4B**). However, the free binding energy of these ligands was generally more positive than those in the first cluster (**Figure 4B**). Meanwhile, seven ligands (1,1,6- trymethyl-1,2-dihydronaphthalene; platycogenic acid B; platycogenic acid A; 12β- hydroxycimigenol; neogogenin acetate; 1α, 2α, 3β, 19α, 23-pentadroxyurs-12-en-28-oic acid-28-o- β-d-xylopyranoside; and tenuifolin) that did not form hydrogen bonds with the four important residues all showed positive free binding energy (**Figure 4C**).

For COX-2, the ten most promising ligands (11-o-p- coumarylnepeticin, nobiletin, fibraurin, dihydroxyeudesm-11 (13)-en-12- oic acid, arteamisinine, genistin, oxypyllenodiol, apigenol, kaempferol, and kirenol) formed at least one hydrogen bond with Ser530, Tyr385, or Arg120 (**Figure 4D**). The following eight ligands (dihydroxyeudesm-11 (13)-en-12- oic acid; pterodontoside; digiprolactone; melazolide; anemonin; robustaflavone; fawcettiine; and terminolic acid) displayed binding poses similar to the native ligand within the COX-2 binding pocket (**Figure 4E**). Conversely, nine ligands (1α, 2α, 3β, 19α, 23-pentadroxyurs-12-en-28-oic-acid-28-o-β-d-xylopyranoside; tenuifolin; neogogenin acetate; 1,1,6-trymethyl-1,2-dihydronaphthalene; platycogenic acid A; platycogenic acid B; 12β- hydroxycimigenol; izalpinin, and pseudosantonim) from the third cluster that failed to establish hydrogen bonds with key residues, resulting in positive binding free energy (**Figure 4F**).

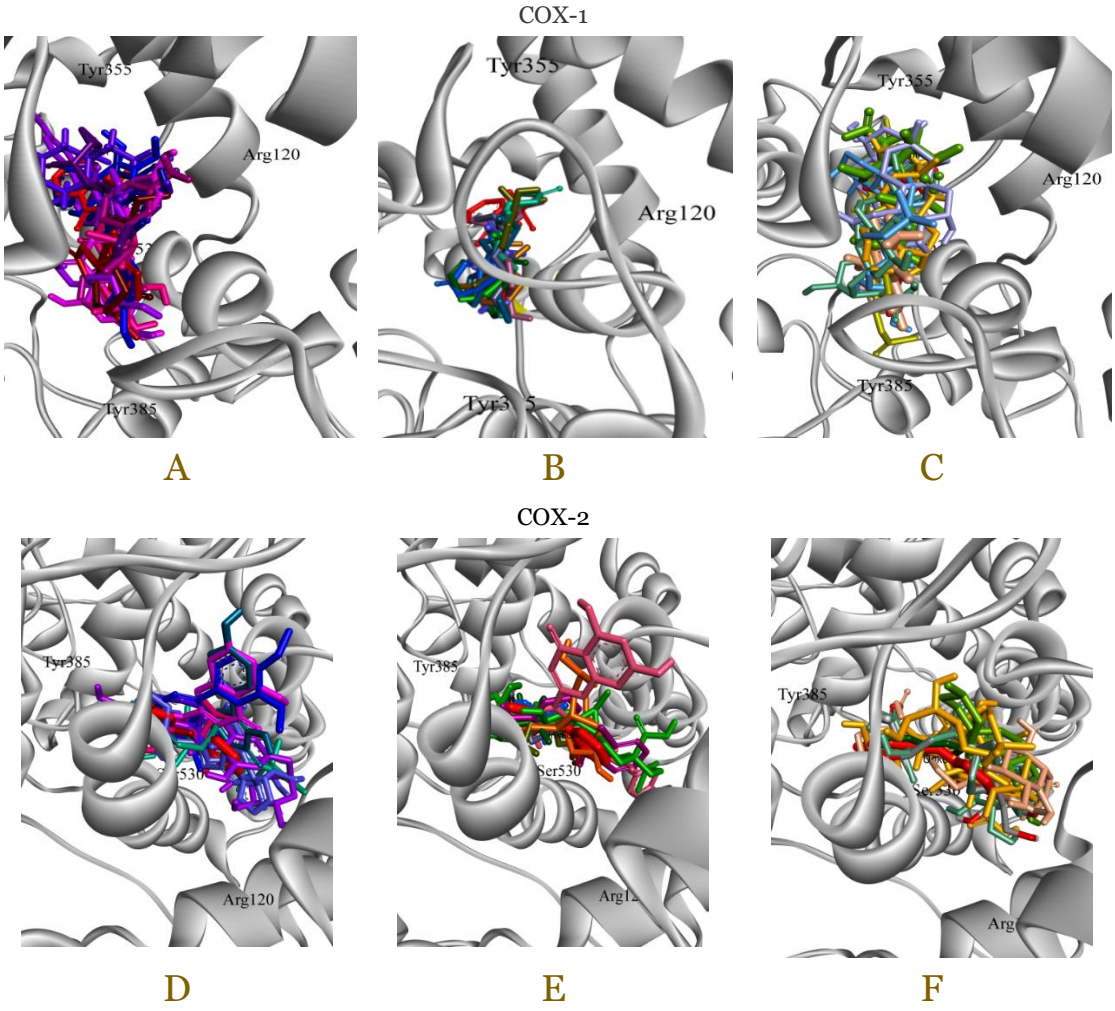

Note:

E1: Dark moss	E8: Sea foam green	E15: Gold	E22: Dark rose
E2: Caribbean blue	E9: Blue	E16: Olive green	E23: Purple
E3: Basil green	E10: Light moss green	E17: Lilac blue	E24: Turquoise
E4: Sienna burnt	E11: Pink	E18: Sky blue	E25: Lilac
E5: Red siena	E12: Marie gold	E19: Maroon	E26: Blue navy
E6: Dark orchid	E13: Tan	E20: Moss pink	E27: Red purple
E7: Forest green	E14: Light lavender	E21: Stone blue	Native ligand: Red

Figure 4. Clustering distribution of docking results from the ethyl acetate ligand against cyclooxygenase-1 (COX-1) (A-C) and cyclooxygenase-2 (COX-2) (D-F) based on binding pose of amino acid residues.

Several non-native ligands displayed higher binding affinity (more negative ΔG values) than the native ligands for COX-1 and COX-2, as demonstrated in **Table 4**. Meloxicam (*ΔG*=-9.50 kcal/mol) and mefenamic acid (*ΔG*=-7.08 kcal/mol) served as reference ligands for COX-1 and COX-2, respectively. Ligand 11-O-p-coumarylnepeticin showed a *ΔG* of -10.44 kcal/mol for COX-1, indicating a stronger binding affinity than meloxicam (**Table 4**). Ligand izalpinin also displayed strong binding affinity, with *ΔG* values of -9.13 kcal/mol for COX-1 and -9.06 kcal/mol for COX-2. Other ligands, such as nobiletin and pseudosantonim, showed notable affinity, with *ΔG* values comparable to meloxicam and superior to mefenamic acid. Conversely, ligands such as fawcettiine and robustaflavone had significantly less favorable binding to COX-1 and failed to interact with COX-2, as indicated by positive or highly unfavorable *ΔG* values. Similarly, ligands platycogenic acid B, platycogenic acid A, and 12-hydroxycimigenol showed positive *ΔG* values for both COX-1 and COX-2, suggesting weak or negligible inhibitory potential. Overall, ligands 11-O-p-coumarylnepeticin and izalpinin emerged as promising candidates for COX-1 and COX-2 inhibition, given their superior binding affinity compared to native ligands.

Table 4. Characteristics of the binding interactions of ligands from the ethyl acetate extract with cyclooxygenase-1 (COX-1) and cyclooxygenase-2 (COX-2) based on molecular docking analysis

Code	Ligand	ΔG (Kcal/mol)	
		COX-1	COX-2
Native ligand	Meloxicam	-9.50	
Native ligand	Mefenamic acid		-7.08
E8	11-O-p-coumarylnepeticin	-10.44	-9.41
E26	Izalpinin	-9.13	-9.06
E9	Nobiletin	-8.83	-8.35
E19	Pseudosantonim	-8.68	-8.46
E6	Fibraurin	-8.64	-6.76
E23	Dihydroxyeudesm-11 (13)-en-12-oic acid	-8.60	-8.08
E5	Arteamisinine	-8.33	-8.03
E27	Pterodontosid	-8.21	-7.25
E25	Genistin	-7.93	-5.37
E20	Oxypyllenodiol A	-7.68	-7.62
E11	Apigenol	-7.48	-7.92
E18	1,1,6-trymethyl-1,2-dihydronaphthalene	-7.27	-6.93
E1	Dihydroactinidiolide	-6.98	-6.64
E24	Kaempferol	-6.81	-7.78
E2	Digiprolactone	-6.75	-6.56
E16	Melazolide A	-6.55	-6.87
E21	Anemonin	-6.36	-6.47
E17	Kirenol	-6.36	-7.48
E4	Fawcettiine	-4.80	-5.14
E22	Robustaflavone	-4.35	19.69
E7	Terminolic acid	-1.56	4.04
E3	Platycogenic acid B	12.61	25.97
E10	Platycogenic acid A	13.63	22.99
E15	12-hydroxycimigenol	13.96	33.47
E14	Neogogenin acetate	14.45	46.29
E12	1α, 2α, 3β, 19α, 23-pentadroxyurs-12-en-28-oic acid-28-o- β-d-xylopyranoside	15.32	34.59
E13	Tenuifolin	51.87	46.37

Δ*G:* binding free energy

Molecular dynamics simulations of ligands from n-hexane extract

Trajectory analysis of the ten selected n-hexane ligands (4,8,12,16-tetramethylheptadecan-4-olide; methyl 3-(3,5-di-tert-butyl-4-hydroxyphenyl)propionate; ((E, E, E))-3,7,11,15-tetramethyl-acetate; 2,6,10,14-Hexadecatetraen-1-ol, 4-(1,1,3,3-tetramethylbutyl)-phenol; 2-Acetoxy-1,1,10-trimethyl-6,9-epidioxydecalin; phytol; farnesyl acetone; β-ionone; 3-4-(2,6,6-trimethyl-2-cyclohexen-1-yl)-buten-2-one; and (E, E))- 6,10-dimethyl-5,9-dodecadien-2-one) with COX-1 and COX-2 demonstrated that all ligands formed interactions with COX-1 and COX-2 (**Figure 5**). However, (E, E)-6,10-dimethyl-5,9-dodecadien-2-one showed a relatively weaker interaction than the others. Leu352 consistently participated in interactions with each tested ligand, followed by Val349 and Ala527, while Met522 and Phe518 showed the least interaction. In the interaction analysis between n-hexane ligands and COX-2, Val349 consistently interacted with each tested ligand. Four ligands—4,8,12,16-tetramethylheptadecan-4-olide, methyl-3-(3,5-di-tert-butyl-4-hydroxyphenyl) propionate, (E, E, E)-3,7,11,15-tetramethyl-acetate, 2,6,10,14-hexadecatetraen-1-ol, and 4-(1,1,3,3-tetramethylbutyl)-phenol—displayed interaction profiles most similar to meloxicam. Overall, this analysis indicated that these four ligands formed stronger interactions compared to the other six ligands tested from the n-hexane extract (**Figure 5**).

Ligand interactions with amino acid residues were analyzed, highlighting differences in bond types, the total number of key and additional significant amino acid residue interactions, and binding free energy (**Table 5** and **Table 6**). The optimal ligands for COX-1 and COX-2 inhibition were evaluated based on the stability of ligand contact conformations with the protein and their binding free energy. Greater conformational stability and more negative binding free energy indicated higher ligand affinity for the protein and greater inhibitory potential for COX. The three top ligands, 4,8,12,16-tetramethylheptadecan-4-olide, methyl 3-(3,5-di-tert-butyl-4-hydroxyphenyl)-propionate, and ((E, E, E))-3,7,11,15-tetramethyl-acetate,2,6,10,14-hexadeca-tetraen-1-ol, demonstrated the highest number of key residues, signifying favorable

conformations for binding with COX-1 (**Table 5**). However, the binding free energy of 2-acetoxy-1,1,10-trimethyl-6,9-epidioxydecalin was more positive than that of the native ligand, leading to its exclusion as a candidate for COX-1 inhibition.

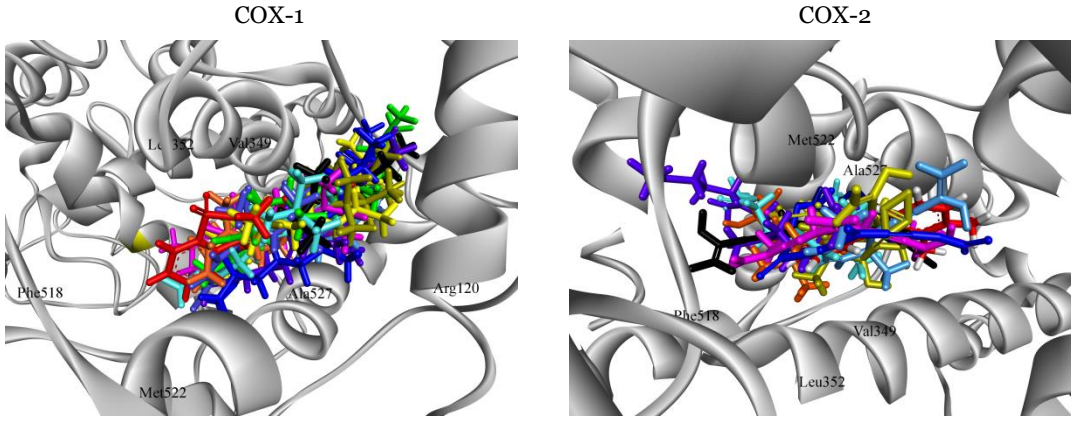

Figure 5. Superimposed of ligands in the binding pocket of cyclooxygenase-1 (COX-1) and cyclooxygenase-2 (COX-2) during molecular dynamics simulation: native ligand (red), 4,8,12,16-tetramethylheptadecan-4-olide (blue), 2-acetoxy-1,1,10-trimethyl-6,9-epidioxydecalin (metallic gray), methyl 3-(3,5-di-tert-butyl-4-hydroxy-phenyl) propionate (cyan), (E, E)-6,10-dimethyl-5,9-dodecadien-2-one (black), β-ionone (corn blue), 4-(1,1,3,3-tetramethylbutyl)-phenol (medium blue), 3-4-(2,6,6-Trimethyl-2-cyclohexen-1-yl)-buten-2-one (orange), farnesyl acetone (purple), ((E, E, E))-3,7,11,15-tetramethyl-acetate, 2,6,10,14-hexadecatetraen-1-ol (hot pink), phytol (green), and hexahydro farnesyl acetone (yellow).

Binding energy analysis using MMPBSA revealed that six ligands (4,8,12,16-tetramethyl-heptadecan-4-olide; methyl 3-(3,5-di-tert-butyl-4-hydroxyphenyl) propionate; ((E, E, E))-3,7,11,15-tetramethyl-acetate, 2,6,10,14-hexadecatetraen-1-ol; phytol; farnesyl acetone, and (E, E))- 6,10-dimethyl-5,9-dodecadien-2-one) had more negative binding energies than the native ligand (**Table 5**). These six compounds shared an aliphatic CH chain structure, which facilitated binding to the COX-1 enzyme through interactions involving π bonds and hydrogen bonds. Among them, methyl 3-(3,5-di-tert-butyl-4-hydroxyphenyl)-propionate; ((E, E, E))-3,7,11,15-tetramethyl-acetate, 2,6,10,14-hexadecatetraen-1-ol; and 4,8,12,16-tetramethyl-heptadecan-4-olide demonstrated the most favorable binding poses (total key and additional amino acid residue interactions) compared to meloxicam. According to MMPBSA calculations, the three ligands with the most negative binding free energy were 4,8,12,16-tetramethylheptadecan-4-olide (ΔG=-41.62 kcal/mol), ((E, E, E))-3,7,11,15-tetramethyl-acetate, 2,6,10,14-hexadecatetraen-1-ol (ΔG=-41.49±0.76 kcal/mol), and phytol (ΔG=-41.41±3.13 kcal/mol). However, phytol was not among the top three COX-1 inhibitors because it lacked strong hydrogen bonds with key residues (Ser530, Arg120**)** and relied mainly on hydrophobic interactions. Although it had a strong binding free energy. Therefore, methyl 3-(3,5-di-tert-butyl-4-hydroxyphenyl) propionate, ((E, E, E))-3,7,11,15-tetramethyl-acetate, 2,6,10,14-hexadeca-tetraen-1-ol, and 4,8,12,16-tetramethyl-hepta-decan-4-olide ranked as the top three ligands for COX-1 inhibition.

Table 5. Results from molecular dynamic simulations: binding free energy and amino acid residues of cyclooxygenase-1 (COX-1) that interact with ligands from n-hexane extract

Code	Ligand	Amino acid residue	TR	ΔG (Kcal/mol)
Native ligand	Meloxicam	Hydrogen bonds (Arg120), Van der Waals (VDW) bonds (Ser353, Tyr355, Ala527), hydrophobic interaction (Ile345, Leu531, Val349, Leu117, Phe518, Ile523, Leu352)	10	-23.95±2.17
H7	4,8,12,16-tetramethylheptadecan-4-olide	Hydrogen Bond (Tyr385), hydrophobic interaction (Arg120, Ala527, Leu531, Ile345, Leu366, Met113, Leu365, Leu534, Leu537, Val116, Leu359, Phe518, Leu352)	8	-41.62±1.03
H3	Methyl 3-(3,5-di-tert-butyl-4-hydroxyphenyl)-propionate	Hydrogen bond (Ser530), VDW (Gly526), hydrophobic interaction (Val349, Ala527, Trp387, Leu352, Phe518)	7	-31.37±3.68

Code	Ligand	Amino acid residue	TR	Δ*G* (Kcal/mol)
H6	(E, E, E)-3,7,11,15-tetramethyl- acetate, 2,6,10,14-Hexadecatetraen-1-ol	Hydrophobic interaction (Ala 202, Tyr348, Trp387, Val349, Phe205, Val344, Leu534, Leu531, Ile345, Leu117, Ile345, Val116, Tyr355)	6	-41.49±0.76
H2	4-(1,1,3,3-tetramethyl-butyl)-phenol	Hydrogen bond (Met522), hydrophobic interaction (Val349, Ala527, Leu352, Gly526, Ile523)	6	-20.46±0.21
H29	2-Acetoxy-1,1,10-trimethyl-6,9-epidioxydecalin	Hydrogen bond (Ser530), VDW (Ala527), hydrophobic interaction (Leu359, Val349, Tyr355, Val116)	5	-22.30±6.56
H4	Phytol	Hydrogen Bond (Asp362), VDW (Lys360, Phe361), hydrophobic interaction (Phe518, Val349, Ala527, Leu352, Leu359, Met113, Leu365, Leu117, Val116, Ile523)	5	-41.41±3.13
H5	Farnesyl acetone	Hydrogen Bond (Tyr385), hydrophobic interaction (Val349, Leu365, Leu117, Met113, Leu359, Val116, Ala527, Leu531)	4	-35.29±4.14
H30	β-Ionone	Hydrophobic interaction (Leu534, Leu531, Val349, Leu359, Ala527, Leu117)	4	-21.60±2.78
H24	3-4-(2,6,6-Trimethyl-2-cyclohexen-1-yl)-buten-2-one	VDW bonds (Ala527), hydrophobic interaction (Leu352, Val349)	3	-20.33±0.99
H12	(E, E))- 6,10-dimethyl-5,9-dodecadien-2-one	Hydrogen bond (Asp362), VDW (Phe361), hydrophobic interaction (Leu117, Met113, Ala116, Tyr355, Leu359)	1	-27.83±0.54

Δ*G:* binding free energy; TR: total key and additional amino acid residues

All ligands containing amino acid residues of COX-2 demonstrated comparable or superior efficacy relative to the native ligand (**Table 6**). The most effective ligands for COX-2 inhibition were characterized by the highest number of key residue interactions and the most negative Δ*G* values across all samples. Binding energy analysis using MMPBSA revealed that six ligands had more negative binding energies than the native ligand. For COX-2, the native ligand, mefenamic acid, had a *ΔG* value of -20.53±2.30 kcal/mol, indicating a relatively stable interaction with COX-2 through hydrophobic interaction with important amino acid residues such as Tyr385, Val349, and Ala527.

Hexahydro farnesyl acetone had the lowest binding free energy (Δ*G*=-42.46±1.13 kcal/mol), indicating the highest affinity for COX-2, with interactions involving 12 amino acid residues (**Table 6**). This stability was supported by hydrogen bond formation with Met522, van der Waals interactions with Gly526, and hydrophobic interactions with residues such as Arg120, Tyr355, Leu352, Val349, Val116, Met113, Leu117, Ile345, Leu531, and Leu359 (**Table 6**). Other ligands, ((E, E, E))- 3,7,11,15-tetramethyl-acetate, 2,6,10,14-hexadecatetraen-1-ol, and 4,8,12,16-tetramethylheptadecan-4-olide, had binding free energies of -33.79±3.80 and -33.05±0.11 kcal/mol, respectively. Thus, 4,8,12,16-tetramethylheptadecan-4-olide, (E, E, E)-3,7,11,15-tetramethyl-acetate, 2,6,10,14-hexadeca-tetraen-1-ol, and hexahydro-farnesyl acetone) were identified as the top three COX-2 inhibitors.

Table 6. Results from molecular dynamic simulations: binding free energy and amino acid residues of cyclooxygenase-2 (COX-2) interact with ligands from n-hexane extract

Code	Ligand	Amino acid residue	TR	Δ*G* (Kcal/mol)
Native ligand	Mefenamic	Hydrophobic interaction (Tyr385, Val349, Phe318, Leu352, Ala527)	4	-20.53±2.30
H7	4,8,12,16-tetramethylheptadecan-4-olide	Hydrogen bonds (Arg120), hydrophobic interaction (Leu352, Val492, Val85, Leu328, Tyr355, Met522, Val349, Trp387, Phe484, Phe174, Tyr385, Phe581, Phe381)	8	-33.05±0.11
H6	(E, E, E)-3,7,11,15-tetramethyl-, acetate, 2,6,10,14-Hexadeca-tetraen-1-ol	Hydrophobic interaction (Val349, Ala527, Tyr355, Val523, His89, Met522, Phe381, Trp387, Phe518, Arg120, Val116)	8	-33.79±3.80
H1	Hexahydrofarnesyl acetone	Hydrogen bonds (Met522), VDW (Gly526), hydrophobic interaction (Arg120, Tyr355, Leu352, Val349, Val116, Met113, Leu117, Ile345, Leu531, Leu359)	7	-42.46±1.13

Code	Ligand	Amino acid residue	TR	ΔG (Kcal/mol)
H12	(E, E))- 6,10-dimethyl-5,9-dodecadien-2-one	Hydrogen bonds (Tyr355, Arg 513), hydrophobic interaction (Ala527, Leu531, Tyr385, Val344, Leu534, Tyr348, Phe205, Leu352, Val349)	6	-21.63±6.35
H30	β-Ionone	Hydrophobic interaction (Val523, Trp387, Met522, Ala527, Val349, Tyr348, Leu352)	6	-15.45±0.98
H24	3-4-(2,6,6-Trimethyl-2-cyclohexen-1-yl)-buten-2-one	Hydrophobic interaction (Leu531, Ala527, Val349, Tyr355, Leu352, Val523)	6	-17.38±1.75
H4	Phytol	Hydrogen bonds (Asp362), VDW (Lys 360, Phe361), hydrophobic interaction (Phe518, Val349, Ala527, Leu352, Met113, Leu359, Leu365, Leu117, Val116, Ile523)	5	-30.89±6.24
H2	4-(1,1,3,3-tetramethyl-butyl)-phenol	Hydrophobic interaction (Ala527, Tyr355, Leu359, Val349, Leu352)	4	-16.55±2.72
H29	2-Acetoxy-1,1,10-trimethyl-6,9-epidioxydecalin	Hydrophobic interaction (Leu352, Val349, Ala527, Val523)	4	-19.43±5.41
H3	Methyl 3-(3,5-di-tert-butyl-4-hydroxyphenyl)-propionate	Hydrogen bonds (Arg120), hydrophobic interaction (Val349, Ala527, Tyr115, Val116)	3	-23.95±5.39

ΔG: binding free energy; TR: total key and additional amino acid residues

Ligand 4,8,12,16-tetramethylheptadecan-4-olide showed minimal fluctuation, with RMSD values remaining ≤3Å (**Figure 6A**). This ligand remained stable throughout the simulation from 0 ns to 200 ns. In contrast, ((E, E, E))-3,7,11,15-tetramethyl-acetate, 2,6,10,14-hexadecatetraen-1-ol, and ((E, E))-6,10-dimethyl-5,9-dodecadien-2-one showed significant fluctuations, with increasing RMSD values observed at 100 ns. However, both ligands stabilized between 125 ns and 200 ns in complex with COX-1 (**Figure 6A**). Hexahydro farnesyl acetone demonstrated a weaker COX-2 inhibitory effect than the other two ligands, as indicated by substantial fluctuations in RMSD values between 25 ns and 125 ns (**Figure 6B**). In contrast, 4,8,12,16-tetramethylheptadecan-4-olide showed minimal fluctuation, maintaining an RMSD value of ≤3Å throughout the 200 ns simulation, similar to ((E, E, E))-3,7,11,15-tetramethyl-acetate and 2,6,10,14-hexadecatetraen-1-ol. These three ligands complexed with COX-2 remained stable throughout the simulation period (**Figure 6B**).

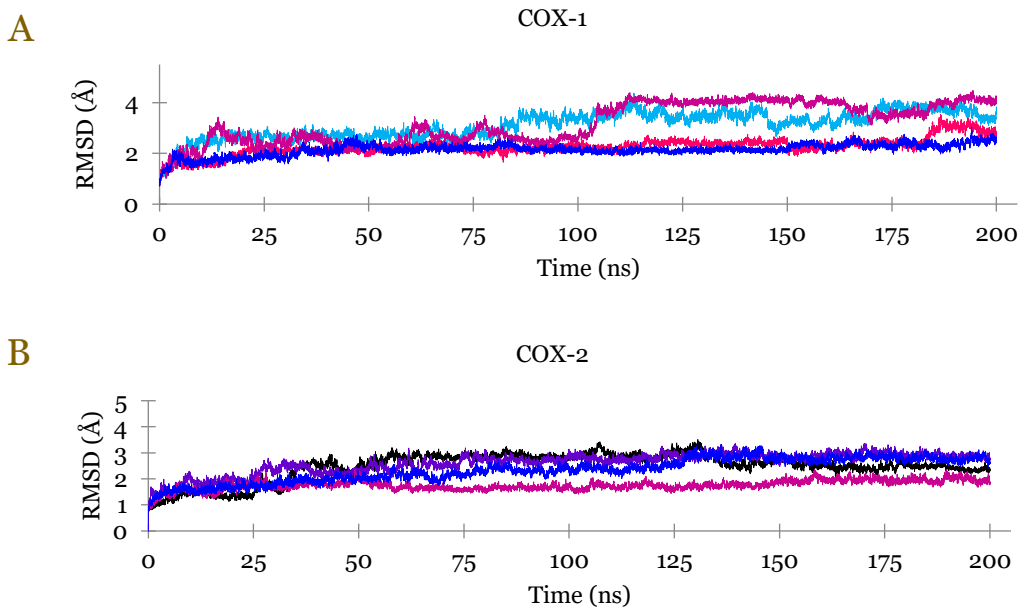

Figure 6. The root mean square deviation (RMSD) of top three ligands (from the n-hexane extract) during interaction with (A) cyclooxygenase-1 (COX-1) and (B) cyclooxygenase-2 (COX-2) in molecular dynamic simulation: meloxicam (red); mefenamic acid (black); hexahydrofarnesyl acetone (purple); methyl 3-(3,5-di-tert-butyl-4-hydroxyphenyl)propionate (cyan): ((E, E, E))-3,7,11,15-tetramethyl-acetate, 2,6,10,14-hexadecatetraen-1-ol (hot pink); 4,8,12,16-tetramethylheptadecan-4-olide (blue).

Molecular dynamics simulations of ligands from ethyl acetate extract

In the trajectory analysis, ten selected compounds from the ethyl acetate extract were evaluated for their interaction with COX-1 and compared to meloxicam as the native ligand. All ten ligands formed bonds with the COX, with interactions primarily dominated by Ala527 and Leu352, while Met522 showed minimal interaction (**Figure 7**). The simulation indicated that izalpinin demonstrated a weaker interaction with COX-1 than the other ligands, as it lacked important amino acid residues essential for binding (**Table 7**). Regarding the interaction between ethyl acetate extract ligands and COX-2, compared to mefenamic acid as the native ligand, the ligands showed similar binding characteristics, with Ala527 consistently involved in the interaction [104]. The simulation further indicated that 11-o-p-coumarylnepeticin had a reduced affinity for COX-2 compared to the other ligands, likely due to the absence of important amino acid residues required for stable binding (**Table 8**).

The ligands pseudosantonin, genistin, and nobiletin demonstrated superior interactions with the COX-1 due to the presence of key residues such as Ser530, Tyr385, and Tyr355 (**Table 7**). Trajectory analysis of the complexes indicated that the binding poses of these compounds were located at the active site of COX-1. In the trajectory analysis of the ethyl acetate extract with COX-2, five complexes—arteaminisine, kaempferol, kirenol, nobiletin, and genistin—demonstrated stronger interactions than the remaining five. These five compounds (arteaminisine, kaempferol, kirenol, nobiletin, and genistin) maintained stable interactions due to the presence of key binding residues, including Arg120, Ser353, Ser530, Tyr385, and Tyr355. Therefore, these ligands could be considered potential inhibitors of COX-2 with analgesic and anti-inflammatory properties.

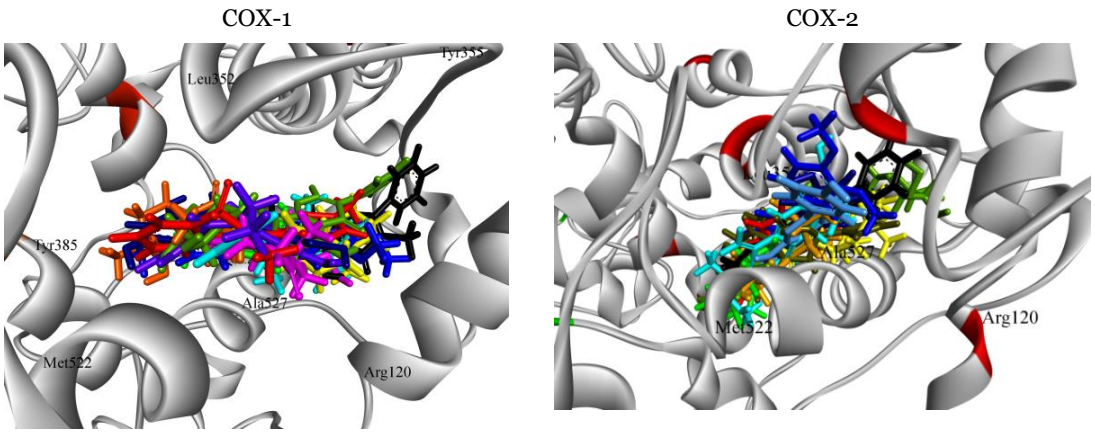

Figure 7. Superimposed ethyl acetate extract ligand with cyclooxygenase-1 (COX-1) and cyclooxygenase-2 (COX-2): native ligand (red), arteamisinine (light sea green), nobiletin (blue), kirenol (cyan), pseudosantonim (pink), dihydroxyeudesm-11 (13)-en-12- oic acid (yellow), kaempferol (corn blue), izalpinin (black), oxxypyllenodiol (orange), pterodontoside (purple), apigenol (navi blue), fibraun (metallic yellow), genisitin (dark blue), and kirenol (cyan).

The molecular dynamics simulation results regarding binding free energy and important amino acid residues interacting with ligands from the ethyl acetate extract against COX-1 and COX-2 enzymes are presented in **Table 7** and **Table 8**. This analysis provided insights into the ligands' stability in binding to the target protein and their selectivity toward COX-1 or COX-2. The simulation results for COX-1 demonstrated variability in binding free energies among the ligands (**Table 7**). Nobiletin had the lowest binding energy (ΔG=-35.20±1.26 kcal/mol), indicating a stronger interaction compared to the native ligand. Meloxicam, as the native ligand, had a ΔG of -23.94±2.17 kcal/mol, which was weaker than pseudosantonin (ΔG=-24.42±1.42 kcal/mol) but stronger than arteamisinine (ΔG=-20.33±2.74 kcal/mol). Pseudosantonin demonstrated greater interactions than nobiletin, forming eight interactions with key amino acids, suggesting a specific and effective affinity for COX-1. Nobiletin was not ranked among the top COX-1 inhibitors despite its strong binding energy (-35.20 kcal/mol) and TR (7) because it did not interact with key catalytic residues (Ser530, Arg120). In contrast, pseudosantonim (-24.42 kcal/mol, TR=8) was selected for its stronger interactions with critical COX-1 sites, making it a more effective inhibitor. Similarly, arteamisinine and genistin showed strong interactions with COX-2, as both formed interactions with eight important amino acid residues. Overall,

pseudosantonim, arteamisinine, and genistin were identified as the top three ethyl acetate ligands with the highest potential to inhibit COX-1.

Table 7. Results from molecular dynamic simulations: binding free energy and amino acid residues of cyclooxygenase-1 (COX-1) that interact with ligands from ethyl acetate extract

Code	Ligand	Amino acid residue	TR	Δ*G* (Kcal/mol)
Native ligand	Meloxicam	Hydrogen bonds (Arg120), Van der Waals (VDW) bonds (Ser353, Tyr355, Ala527), hydrophobic interaction (Ile345, Leu531, Val349, Leu117, Phe518, Ile523, Leu352)	10	-23.94±2.17
E19	Pseudosantonim	Hydrogen bonds (Arg120, Val116), VDW (Ser530), hydrophobic interaction (Leu534, Ile345, Leu352, Val349, Tyr355, Ala527)	8	-24.42±1.42
E5	Arteamisinine	Hydrogen bonds (Arg120), hydrophobic interaction (Leu352, Ile523, Ala527, Ile345, Leu534, Val349, Leu531)	8	-20.33±2.74
E25	Genistin	Hydrogen bonds (Ser530, Met522, Lys 360), sulfur bonds (Met113), VDW (Ser353, His90, Ala527, Leu352, Ile523, Gly526), hydrophobic interaction (Ile345, Val349, Leu531).	8	-13.53±2.51
E9	Nobiletin	Hydrogen bonds (Tyr385), hydrophobic interaction (Val349, Leu359, Leu 351, Leu 354, Ile345, Gly526, Leu352, Ala527)	7	-35.20±1.26
E11	Apigenol	Hydrogen bonds (Met522, Tyr385), VDW (Ser530), hydrophobic interaction (Ala 349, Ala527, Leu352, Gly526)	7	-19.41±0.98
E20	Oxypyllenodiol A	Hydrogen bonds (Ser530, Ala527, Met522, Tyr385), hydrophobic interaction (Ile523, Leu352, Phe518, Hie 90)	7	-18.82±0.60
E27	Pterodontoside	Hydrogen bonds (Val116), VDW (Leu352), hydrophobic interaction (Ile523, Val349, Ala527, Gly526)	5	-23.47±0.38
E6	Fibraurin	Hydrogen bonds (Ser530), VDW (His90, Leu117), hydrophobic interaction (Val349, Ile345, Ala527, Ile523)	5	-18.17±2.74
E23	Dihydroxyeudesm-11 (13)-en-12- oic acid	VDW (Ser530, Ala527), hydrophobic interaction (Val349, Leu359, Ile345, Met113, Leu531, Leu117, Leu534, Leu535)	5	-24.41±1.32
E26	Izalpinin	VDW (Ser530), hydrophobic interaction (Val349, Leu117, Met113, Ile345, Leu531)	4	-26.29±2.93

Δ*G:* binding free energy; TR: total key and additional amino acid residues

Nobiletin had the lowest binding free energy (Δ*G*=-31.10±0.15 kcal/mol), confirming its strong binding affinity in COX-2, as presented in **Table 8**. Other ligands, such as kaempferol and arteamisinine, also demonstrated high affinity for COX-2, with Δ*G* values of -23.39± 2.76 kcal/mol and -23.54±0.30 kcal/mol, respectively. Mefenamic acid, the native ligand for COX-2, had a Δ*G* of -20.53±2.30 kcal/mol, which was higher than several ligands from the ethyl acetate extract. In terms of key amino acid interactions, arteamisinine demonstrated the highest number of interacting residues among all ligands, forming nine interactions, while kaempferol, fibraun, and apigenol each demonstrated eight interactions. Arteamisinine engaged with two important amino acid residues and seven active residues, signifying its potent and unique affinity for COX-2 (**Table 8**). Key residues involved in COX-2 interactions included Tyr385, Ala527, Leu352, and Val349 (**Table 8**). The majority of interactions were dominated by hydrogen bonding, hydrophobic interactions, and van der Waals forces.

Table 8. Results from molecular dynamic simulations: binding free energy and amino acid residues of cyclooxygenase-2 (COX-2) that interact with ligands from ethyl acetate extract

Code	Ligand	Amino acid residue	TR	Δ*G* (Kcal/mol)
Native ligand	Mefenamic acid	Hydrophobic interaction (Tyr385, Val349, Phe318, Leu352, Ala527)	4	-20.53±2.30
E5	Arteamisinine	Hydrogen bonds (Ser530, Tyr385), hydrophobic interaction (Val349, Ala527, Leu352, Val523, Trp387, Phe518, Met522)	9	-23.54±0.30

Code	Ligand	Amino acid residue	TR	ΔG (Kcal/mol)
E24	Kaempferol	Hydrogen bonds (Ser353), VDW (Ser530), hydrophobic interaction (Tyr355, Ala 516, Val523, Leu352, Ala527, Gly526)	8	-23.39±2.76
E6	Fibraurin	VDW (Ser353, His90, Ser530), hydrophobic interaction (Val349, Leu352, Tyr348, Val523, Ala527, Leu531, Arg120)	8	-19.29±3.35
E11	Apigenol	Hydrogen bonds (Tyr355), VDW (Ser353, Tyr385), hydrophobic interaction (Val349, Val523, Ala527, Leu352, Gly526).	8	-16.48±0.57
E17	Kirenol	Hydrogen bonds (Trp387, Met522), hydrophobic interaction (Val523, Ala527, Leu352, Tyr355, Phe518)	7	-28.46±0.62
E20	Oxypyllenodiol A	Hydrogen bonds (Ser530, Met522, Val523), VDW (Gly526), hydrophobic interaction (Leu352, Ala527, Tyr355)	7	-19.20±0.68
E9	Nobiletin	Hydrogen bonds (Ser530), sulphuric acid (Arg 513), hydrophobic interaction (Leu352, Val523, Ala527, Val349, Leu531)	6	-31.10±0.15
E25	Genistin	Hydrogen bonds (Tyr 233), VDW (Trp387, Val116), hydrophobic interaction (Phe518, Val523, Leu531, Ala527, Val349)	6	-23.18±4.57
E23	Dihydroxyeudesm-11 (13)-en-12- oic acid	VDW (Val523, Gly526), hydrophobic interaction (Ala527, Arg120, Val116, Val349, Leu534, Leu531)	6	-23.39±2.76
E8	11-O-p- Coumaryl-nepeticin	VDW (Pro 300), hydrophobic interaction (Tyr355, Lys135, Val134)	1	-19.29±3.35

ΔG: binding free energy; TR: total key and additional amino acid residues

The COX-1 graph demonstrated that pseudosantonim demonstrated minimal fluctuation, with an RMSD value of ≤3Å, maintaining stability from 25 ns to 200 ns during the simulation (**Figure 8A**). Genistin showed a decline at 150 ns before stabilizing immediately until 200 ns, whereas arteamisinine demonstrated fluctuations between 150 ns and 200 ns. The COX-2 graph indicated that arteamisinine, fibraun, and kaempferol maintained relative stability from 25 ns to 200 ns, with RMSD values of ≤3Å (**Figure 8B**). These three ligands had stable binding to COX-2 throughout the simulation, suggesting their potential as stable COX-2 inhibitors.

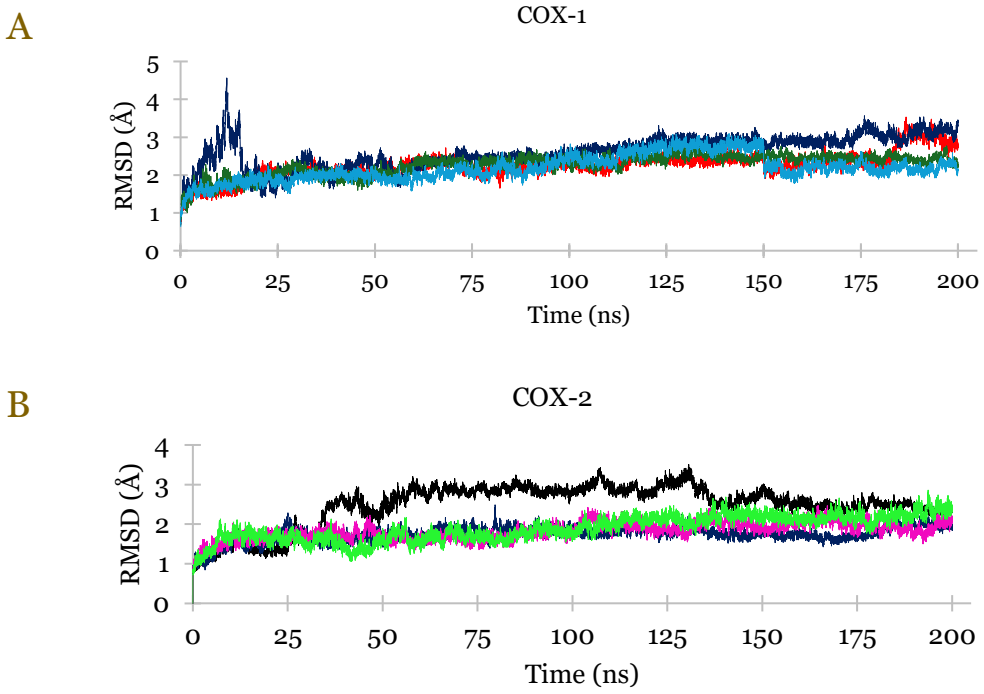

Figure 8. The root mean square deviation (RMSD) of top three ligands (ethyl acetate extract) during interaction with (A) cyclooxygenase-1 (COX-1) and (B) cyclooxygenase-2 (COX-2) in molecular dynamic simulation. Meloxicam (red); mefenamic acid (black); arteamisinine (blue); pseudosantonim (green); genistin (forest green); fibraurin (pink); kaempferol (light green).

Analysis of the selection of the best ligands as COX-1 and COX-2 inhibitors

The simulation trajectory of 4,8,12,16-tetramethylheptadecan-4-olide (from n-hexane extract) and pseudosantonim (from ethyl acetate extract) against COX-1 revealed that pseudosantonim exited the COX-1 binding pocket at 50 ns (**Figure 9**). However, by 100–200 ns, the ligand had stabilized within the binding pocket. Based on binding interactions, MMPBSA analysis, and RMSD graphs from the COX-1 molecular dynamics simulation complex, 4,8,12,16-tetramethylheptadecan-4-olide demonstrated greater inhibitory potential against COX-1 than pseudosantonim, as indicated by its stronger binding affinity (ΔG=-41.62±1.03 kcal/mol) compared to pseudosantonim (ΔG=-24.42±1.42 kcal/mol). Therefore, 4,8,12,16-tetramethylheptadecan-4-olide was identified as the most effective COX-1 inhibitor among the ligands derived from *L. decumana*.

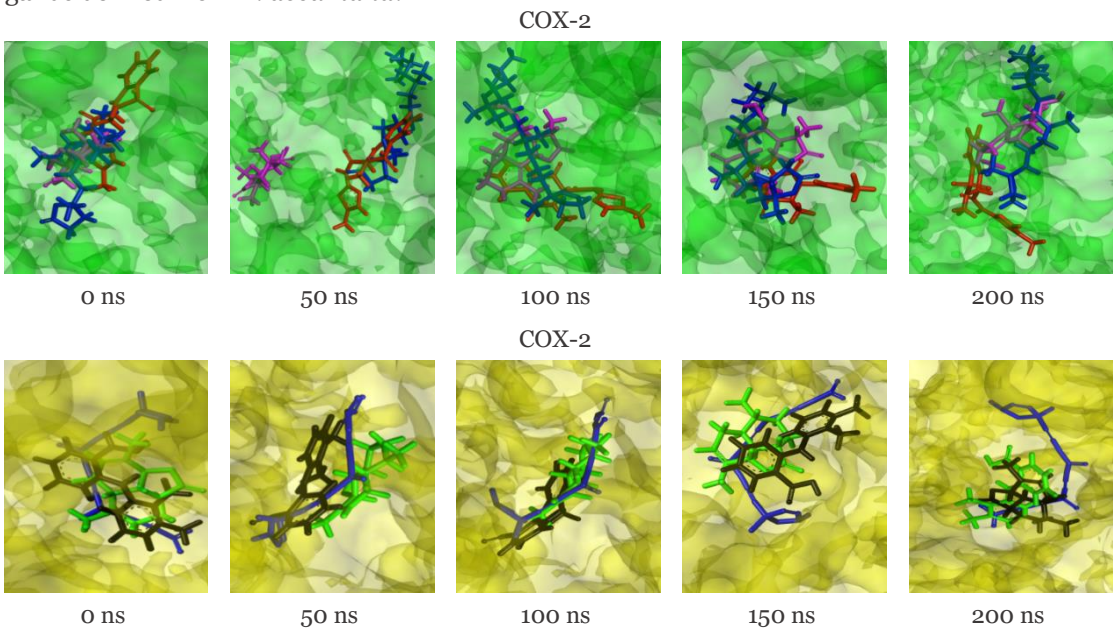

Figure 9. The trajectory of native ligands and the studied ligands during 200 ns molecular dynamics (MD) simulation in the binding site of cyclooxygenase-1 (COX-1) and cyclooxygenase-2 (COX-2). Meloxicam: red; 4,8,12,16-tetramethylheptadecan-4-olide (COX-1): blue; pseudoxantonim: pink; mefenamic acid: black; 4,8,12,16-tetramethylheptadecan-4-olide (COX-2): blue; arteamisinine: green.

For COX-2, the trajectory simulation of 4,8,12,16-tetramethylheptadecan-4-olide (from n-hexane extract) and arteamisinine (from ethyl acetate extract) demonstrated that both ligands remained within the COX-2 binding pocket throughout the simulation (**Figure 9**). Based on binding interactions, MMPBSA analysis, and RMSD graphs from the molecular dynamics simulation of the COX-2 ligand complex, arteamisinine was identified as the most effective COX-2 inhibitor compared to 4,8,12,16-tetramethylheptadecan-4-olide. Arteamisinine interacted with nine important amino acid residues of COX-2, forming two hydrogen bonds (Ser530, Tyr385) and seven hydrophobic interactions (Val349, Ala527, Leu352, Val523, Trp387, Phe518, Met522). In contrast, 4,8,12,16-tetramethylheptadecan-4-olide formed a single hydrogen bond (Arg120) and seven hydrophobic interactions (Leu352, Val492, Val85, Leu328, Tyr355, Met522, Val349, Trp387, Phe484, Phe174, Tyr385, Phe581, Phe381). The ligand binding profile over the 200 ns simulation indicated that arteamisinine consistently maintained its binding at the same COX-2 site. Thus, arteamisinine was identified as the most promising COX-2 inhibitor among the ligands derived from *L. decumana*.

Discussion

The interaction of meloxicam with COX-1 during molecular docking and molecular dynamics simulations demonstrated that the thiazole group formed alkyl bonds with Ile345, Leu535, Leu531, Leu534, and Val349. The carboxamide carbonyl group engaged in hydrogen bonding with Ser353, His90, and Ser530, while the carboxamide amide group formed a hydrogen bond

with Tyr355. Additionally, the benzene group had a stacked amide–π interaction with Met522, and alkyl interactions were observed with Leu352 and Ile523 [34,104,105]. In the interaction of mefenamic acid with COX-2, the hydrogen atom in the phenyl group formed an alkyl bond with Val346, while the hydrogen atom in the benzoic acid group formed a π bond with Leu 349, Ala 523, and Val 520 [14,40]. Another study reported that the N-thiazole group of meloxicam established hydrogen bonds with Tyr385 and Ser530, whereas the carboxamide carbonyl group formed hydrogen bonds with Tyr355 and Arg120 [40]. The binding pose of meloxicam in the COX-1 active site closely resembled that in COX-2, further validating the accuracy of docking predictions in both enzyme models [106].

This study demonstrated that COX-1 complexed with ligands from n-hexane extracts showed a distinct interaction pattern. The complex formed with 4,8,12,16-tetramethylheptadecan-4-olide showed a more negative binding free energy than meloxicam, whereas other ligands did not interact with important amino acid residues in the docking simulation. Ligand binding to COX-2 involved interactions with amino acid residues that were consistent with key residues identified in a previous study [33].

This study evaluated the binding interactions from the docking of meloxicam and various ligands from the ethyl acetate extract with COX-2. The native ligand, mefenamic acid, showed a binding affinity of –7.08 kcal/mol. However, several ligands from the ethyl acetate extract demonstrated more negative binding free energies than the native ligand. These ligands were excluded from the molecular dynamics simulation due to their lack of interaction with important amino acid residues of COX-2. The molecular interactions primarily involved hydrogen bonds and hydrophobic interactions, with electrostatic interactions contributing significantly to ligand-protein affinity. This structural characteristic facilitated interactions with selective COX-2-specific molecules, supporting the development of selective nonsteroidal anti-inflammatory drugs with reduced gastrointestinal side effects.

The interactions between n-hexane extract ligands and COX-2 in this study identified Val349 as a consistently involved residue. The selection of the optimal n-hexane and ethyl acetate extract ligand was based on binding affinity and interactions with key COX amino acid residues. Among the ten n-hexane extract ligands analyzed, four demonstrated superior interactions compared to the others. Among these, 4,8,12,16-tetramethylheptadecan-4-olide demonstrated the strongest interaction with both COX-1 and COX-2, making it the most promising ligand. Similarly, ligands from the ethyl acetate extract showed comparable interactions with COX-2, with arteamisinine displaying the highest binding affinity. While apiol and dihydroxyeudesm-11(13)-en-12-oic acid showed relatively stable interactions, arteamisinine demonstrated the most favorable binding to COX-2. The study concluded that arteamisinine was the most potent COX-2-interacting ligand, with promising potential as an analgesic and anti-inflammatory agent.

This study provided significant pharmacological insights into the development of anti-inflammatory and analgesic agents targeting COX-1 and COX-2 enzymes. A key finding was the traditional use of *L. decumana* leaves as a pain reliever by ethnopharmacologists. The active compounds from this plant demonstrated COX-1 and COX-2 inhibitory properties, a novel finding that has not been previously documented. The study's conclusions were based on ligand selectivity and the binding affinity of ligand-COX complexes, which demonstrated significant activity. Among the identified compounds, 4,8,12,16-tetramethylheptadecan-4-olide emerged as the most potent COX-1 inhibitor, with an exceptional binding free energy (ΔG=-41.62 kcal/mol) and stable interactions with important residues (Arg120, Tyr385, and Ser530). These findings suggested that 4,8,12,16-tetramethylheptadecan-4-olide may serve as a highly selective COX-1 inhibitor with superior potency compared to meloxicam. Additionally, arteamisinine was identified as the most promising COX-2 inhibitor, forming persistent hydrogen bonds with Ser530 and Tyr385, along with hydrophobic interactions with other amino acid residues. Its enhanced binding affinity suggested its potential as a viable alternative to mefenamic acid.

The structural interactions within the complex indicated that hydrogen bond and hydrophobic interactions predominated in ligand-enzyme binding, while electrostatic interactions further enhanced ligand affinity. These findings aligned with the molecular interaction characteristics of established COX inhibitors such as meloxicam and mefenamic acid. In terms of molecular dynamics and stability, 4,8,12,16-tetramethylheptadecan-4-olide and

arteamisinine demonstrated RMSD values below 3 Å, indicating sustained structural stability throughout 200 ns simulations, which was considered optimal. The persistent binding of 4,8,12,16-tetramethylheptadecan-4-olide, for COX-1, and arteamisinine, for COX-2, suggested a robust inhibitory profile with minimal structural variation. This study identified essential residues (Arg120, Ser530, Tyr355, Tyr385) critical for effective COX inhibition, along with the crucial binding conformations of the ligand-protein complexes. Both 4,8,12,16-tetramethylheptadecan-4-olide and arteamisinine effectively engaged with these residues, highlighting their pharmacological potential. The structure-activity relationships (SARs) of these ligands, characterized by specific structural attributes such as aliphatic CH chains that facilitate π and hydrogen bond, suggested enhanced binding affinity. These findings provided a foundation for optimizing ligand structures to improve COX selectivity and efficacy.

This study identified both consistencies and discrepancies with existing literature. The findings supported previous research by confirming that key residues (Arg120, Ser530, Tyr355, Tyr385) and predominant interaction types (hydrogen bonding, hydrophobic interaction) aligned with established COX inhibitors such as meloxicam and mefenamic acid [33]. These results reinforced prior conclusions regarding the kinetics of COX ligand binding [107]. Additionally, the RMSD values provided a critical indicator of structural stability, consistent with accepted methodologies in molecular dynamics research [33]. However, this study also revealed notable deviations from prior research [108]. Ligands such as 4,8,12,16-tetramethylheptadecan-4-olide and arteamisinine demonstrated superior binding conformations and stability compared to conventional COX inhibitors, suggesting that naturally derived ligands may offer greater potency and selectivity than synthetic counterparts. Furthermore, the emphasis on aliphatic chain-based ligands with π-bonding potential diverged from conventional drug design approaches, which often prioritize aromaticity and rigid frameworks [109]. The exclusion of high-affinity ligands, such as 11-O-p-coumarylnepeticin, due to inadequate interactions with canonical residues contrasted with investigations into non-classical binding pathways and allosteric sites, highlighting potential alternative mechanisms of COX inhibition.

A primary limitation of this study was the exclusion of ligands with significant binding free energies. Several ligands with highly negative binding free energies, such as 11-O-p-coumarylnepeticin, were omitted due to insufficient interactions with important residues. While this criterion was justifiable, it highlighted the need for further investigation into alternative binding sites or allosteric inhibitory mechanisms. Another limitation was the reliance on computational docking and molecular dynamics simulations without experimental validation. Enzyme inhibition assays or in vivo studies are essential to confirm the pharmacological relevance of these findings. Additionally, the study focused solely on known binding residues, specifically Arg120, Ser530, Tyr355, and Tyr385. Although these residues are widely recognized as key interaction sites, other potential binding sites or non-canonical interactions remain underexplored. This limitation may have led to the exclusion of ligands with novel binding strategies.

Future directions from this study emphasize the need for experimental validation through both in vitro and in vivo investigations to assess the pharmacokinetics, safety, and efficacy of 4,8,12,16-tetramethylheptadecan-4-olide, arteamisinine, and other promising ligands. Optimization of the SAR is essential to refine ligand architecture based on identified critical interactions, thereby enhancing selectivity and reducing off-target effects. Furthermore, this study suggests exploring allosteric inhibition by analyzing ligands previously excluded due to their lack of interaction with important amino acid residues at canonical binding sites but showing high binding free energy. Lastly, the potential for combination therapy should be investigated, evaluating the synergistic effects of multiple ligands to achieve dual COX-1/COX-2 inhibition while minimizing adverse effects.

Conclusion

In the n-hexane extract of *Laportea decumana* (Roxb.) Wedd., 31 compounds were identified by GC-MS. In silico studies revealed that 10 of these compounds showed the best interactions in docking simulations and remained stable in the protein's binding pocket during molecular dynamics simulations. Among these, 4,8,12,16-tetramethylheptadecan-4-olide demonstrated

stable binding with both COX-1 and COX-2, with binding free energies of -41.62±1.03 kcal/mol and -33.05±0.11 kcal/mol, respectively. In the ethyl acetate extract, 27 compounds were identified by LC-MS, and 10 showed the best interactions in docking simulations, maintaining stability in the protein's binding pocket during molecular dynamics simulations. Pseudosantonim demonstrated better affinity for COX-1 (-24.41±1.32 kcal/mol), while arteamisinine had a higher affinity for COX-2 (-23.53±0.30 kcal/mol). These findings suggest that 4,8,12,16-tetramethylheptadecan-4-olide was the most effective COX inhibitor in the n-hexane extract, while pseudosantonim and arteamisinine merit further investigation as potential COX-1 and COX-2 inhibitors, respectively, in the ethyl acetate extract. This study concluded that 4,8,12,16-tetramethylheptadecan-4-olide was the most potent COX-1 inhibitor, whereas arteamisinine was the most effective for COX-2 inhibition.

Ethics approval

Not required.

Acknowledgments

The ESS acknowledges *Beasiswa Pendidikan Indonesia* (BPI) for the doctoral study scholarship (ID number 202101121682); *Pusat Pelayanan Pembiayaan dan Asesmen Pendidikan Tinggi* (PPAPT), Ministry of Higher Education, Science, and Technology of Republic Indonesia doctoral study, and *Lembaga Pengelola Dana Pendidikan* (LPDP), Ministry of Finance of the Republic of Indonesia for supporting publication.

Competing interests

The authors declare that there are no competing interests.

Funding

This study received was funded by Lembaga Pengelola Dana Pendidikan (LPDP), the Ministry of Finance of the Republic of Indonesia.

Underlying data

Derived data supporting the findings of this study are available from the corresponding author on request.

Declaration of artificial intelligence use

This study used artificial intelligence (AI) tool and methodology of which AI-based language model ChatGPT was employed in the language refinement (improving grammar, sentence structure, and readability of the manuscript). We confirm that all AI-assisted processes were critically reviewed by the authors to ensure the integrity and reliability of the results. The final decisions and interpretations presented in this article were solely made by the authors.

How to cite

Simaremare ES, Kurniawan F, Hartati R, Tjahjono DH. Exploring the potential of *Laportea decumana* extract compounds as COX-1 and COX-2 inhibitors: An in silico study. Narra J 2025; 5 (1): e1627 - http://doi.org/10.52225/narra.v5i1.1627.

References

1. Simaremare ES, Gunawan E, Alua O. Active compounds characteristics and test leaf extract anticholesterol itchy leaf [*Laportea decumana* (Roxb.) Wedd.]. Int J Pharm Res 2020;12(3):1310-1315.
2. Simaremare ES, Gunawan E, Yarangga I, *et al.* Antibacterial and toxicity activities itchy leaves (*Laportea decumana*, Roxb. Wedd) extract. J Phys Conf Ser 2020;1503(1):012041.
3. Simaremare ES, Gunawan E, Yabansabra YR. Evaluation of pharmacological activities of itchy leaf extracts (*Laportea decumana* (Roxb.) Wedd.). Int J Pharm Res 2020;12(3):1316-1327.

4. Simaremare ES, Fadhilah RF, Gunawan E, *et al.* Anticoagulant activity of ethanolic extract stingging nettle from Biak Numfor. Trends Pharm Nanotechnol 2019;1(1):35-43.
5. Simaremare ES, Tolip MRY, Pratiwi RD. Formulation and effectiveness test of analgesic patch from itchy leaves (*Laportea decumana* (Roxb.) Wedd). Curr Appl Sci Technol 2022;22(3):1-13.
6. Basy LL, Santosa D, Murwanti R, *et al.* Uncover itchy leaves ethnomedicine usage: A preliminary study on characterization and bioactivity of *Laportea* spp. Pharmacogn J 2022;14(4):286-295.
7. Schneider C, Pratt DA, Porter NA, *et al.* Control of oxygenation in lipoxygenase and cyclooxygenase catalysis. Chem Biol 2007;14(5):473-488.
8. Vishwakarma RK, Negi DS. The develompment of COX-1 and COX-2 inhibitors: A review. IJPSR 2022;11(8):3544-3555.
9. Cronstein BN. Cyclooxygenase-2-selective inhibitors: Translating pharmacology into clinical utility. Cleve Clin J Med 2002;69 Suppl 1:SI13-SI19.
10. Aziz MA, Mehedi M, Akter MI, *et al.* In vivo and in silico evaluation of analgesic activity of *Lippia alba*. Clin Phytoscience 2019;5(1):38.
11. Seth B. Non-opioid analgesics. Anaesth Intensive Care Med 2019;20(8):456-459.
12. Hanna VS, Hafez EAA. Synopsis of arachidonic acid metabolism: A review. J Adv Res 2018;11:23-32.
13. Faki Y, Er A. Different chemical structures and physiological/pathological roles of cyclooxygenases. Rambam Maimonides Med J 2021;12(1):e0003.
14. Rouzer CA, Marnett LJ. Structural and chemical biology of the interaction of cyclooxygenase with substrates and non-steroidal anti-inflammatory drugs. Chem Rev 2020;120(15):7592-7641.
15. Bell A. The neurobiology of acute pain. Vet J 2018;237:55-62.
16. Yam MF, Loh YC, Tan CS, *et al.* General pathways of pain sensation and the major neurotransmitters involved in pain regulation. Int J Mol Sci 2018;19(8):2164.
17. Ahmed F, Samantasinghar A, Soomro AM, *et al.* A systematic review of computational approaches to understand cancer biology for informed drug repurposing. J Biomed Inform 2023;142:104373.
18. Lukman LB, Hertiani T, Murwanti R, *et al.* Investigation of Cox-2 inhibition of *Laportea decumana* (Roxb). Wedd extract to support its analgesic potential. J Ethnopharmacol 2024;318(Pt A):116857.
19. Simaremare ES. Skrining fitokimia ekstrak etanol daun gatal (*Laportea decumana* (Roxb.) Wedd). Pharmacy 2014;11(01):98-107.
20. ACD Labs. ACD/ChemSketch version 4.5 for Microsoft Windows. Toronto: Advanced Chemistry Development; 2000.
21. Morris GM, Goodsell DS, Pique ME, *et al.* AutoDock version 4.2: User guide. La Jolla: Scripps Research Institute: 2010.
22. Sanner MF. Python: A programming language for software integration and development. J Mol Graph Model 1999;17(1):57-61.
23. Case DA, Betz RM, Cerutti DS, *et al.* AMBER 2016. San Francisco: University of California; 2016.
24. Pettersen EF, Goddard TD, Huang CC, *et al.* UCSF Chimera - a visualization system for exploratory research and analysis. J Comput Chem 2004;25(13):1605-1612.
25. Hanwell MD, Curtis DE, Lonie DC, *et al.* Avogadro: An advanced semantic chemical editor, visualization, and analysis platform. J Cheminform 2012;4:17.
26. Biovia. Biovia Discovery Studio® 2020: Comprehensive modeling and simulations for life sciences datasheet. Vélizy-Villacoublay: Dassault Systèmes; 2020.
27. Dauber C, Carreras T, González L, *et al.* Characterization and incorporation of extracts from olive leaves obtained through maceration and supercritical extraction in Canola oil: Oxidative stability evaluation. LWT 2022;160:113274.
28. Alkandahri MY, Maulana YE, Subarnas A, *et al.* Antimalarial activity of extract and fractions of *Cayratia trifolia* (L.) Domin. Int J Pharm Res 2020;12:1435-1441.
29. Agilent Technologies. MassHunter personal compound database and library manager: Quick start guide. Santa Clara: Agilent Technologies; 2024.
30. Orlando BJ, Malkowski MG. Substrate-selective inhibition of cyclooxygeanse-2 by fenamic acid derivatives is dependent on peroxide tone. J Biol Chem 2016;291(29):15069-15081.
31. Rayan B, Rayan A. Avogadro program for chemistry education: To what extent can molecular visualization and three-dimensional simulations enhance meaningful chemistry learning? World J Chem Educ 2017;5(4):136-141.
32. Morris GM, Goodsell DS, Halliday RS, *et al.* Automated docking using a Lamarckian genetic algorithm and an empirical binding free energy function. J Comput Chem 1998;19(14):1639-1662.

33. Akaho E, Fujikawa C, Runion HI, *et al.* A study on binding modes of nonsteroidal anti-inflammatory drugs to COX1 and COX2 as obtained by Dock4.0. J Chem Softw 1999;5(4):147-162.
34. Farag DB, Farag NA, Esmat A, *et al.* Synthesis, 3D pharmacophore, QSAR and docking studies of novel quinazoline derivatives with nitric oxide release moiety as preferential COX-2 inhibitors. MedChemComm 2015;6(2):283-299.
35. Meng XY, Zhang HX, Mezei M, *et al.* Molecular docking: A powerful approach for structure-based drug discovery. Curr Comput Aided-Drug Des 2012;7(2):146-157.
36. Naqvi AAT, Mohammad T, Hasan GM, *et al.* Advancements in docking and molecular dynamics simulations towards ligand-receptor interactions and structure-function relationships. Curr Top Med Chem 2019;18(20):1755-1768.
37. Ahmad S, Singh S, Srivastava MR, *et al.* Molecular docking simplified: Literature review. Adv Med Dent Health Sci 2022;4(4):37-44.
38. Miller BR, McGee TD, Swails JM, *et al.* MMPBSA.py: An efficient program for end-state free energy calculations. J Chem Theory Comput 2012;8(9):3314-3321.
39. Sun H, Li Y, Shen M, *et al.* Assessing the performance of MM/PBSA and MM/GBSA methods. 5. Improved docking performance using high solute dielectric constant MM/GBSA and MM/PBSA rescoring. Phys Chem Chem Phys 2014;16(40):22035-22045.
40. Oniga SD, Pacureanu L, Stoica CI, *et al.* COX inhibition profile and molecular docking studies of some 2-(trimethoxyphenyl)-thiazoles. Molecules 2017;22(9):1507.
41. Balogun OS, Ajayi OS, Adeleke AJ. Hexahydrofarnesyl acetone-rich extractives from *Hildegardia barteri*. J Herbs Spices Med Plants 2017;23(4):393-400.
42. Aziz AHA, Engliman NS, Mansor MF, *et al.* Extraction of phenolic compound using natural deep eutectic solvent from biomass waste. IOP Conf Ser Mater Sci Eng 2021;1192(1):012001.
43. Li X, Wang ZG, Chen HH, *et al.* The antioxidant methyl 3-(3,5-di-tert-butyl-4-hydroxyphenyl)propionate. Acta Crystallogr Sect C Struct Chem 2014;70(Pt 11):1050-1053.
44. Gutbrod K, Romer J, Dörmann P. Phytol metabolism in plants. Prog Lipid Res 2019;74(2018):1-17.
45. Nugroho LH, Lexinta EC, Priyono Y, *et al.* Short communication: Composition of terpenoid compounds in essential oils extracted from stems of eight *Piper* species and their role in taxonomic relationships. Biodiversitas 2020;21(8):3438-3443.
46. Syamsudin TS, Hafsah H, Iriawati I. Data set on volatile compound of coffee flowers at different annual rainfall. Data Brief 2019;26:104418.
47. Pratama OA, Tunjung WAS, Sutikno, *et al.* Bioactive compound profile of melon leaf extract (*Cucumis melo* l. 'Hikapel') infected by downy mildew. Biodiversitas 2019;20(11):3448-3453.
48. Rufai Y, Basar N, Sani A. Optimization and isolation of 4,8,12,16-tetramethylheptadecan-4-olide from *Deinbollia pinnata*. Asian J Chem 2019;31(11):2503-2511.
49. Zhou Y, Liang H, Wang Z, *et al.* Clionaterpene, a new cadinene sesquiterpene from the marine sponge *Cliona* sp. J Mar Sci Eng 2023;11(1):131.
50. Parbuntari H, Etika SB, Mulia M. Identification and prediction of potential drug-like compounds from ruku-ruku leaves (*Ocimum tenuiflorum* Linnen) in West Sumatera. Adv Biol Sci Res 2020;10:248-252.
51. Daba GM, Elkhateeb WA, El-Dein AN, *et al.* Therapeutic potentials of n-hexane extracts of the three medicinal mushrooms regarding their anti-colon cancer, antioxidant, and hypocholesterolemic capabilities. Biodiversitas 2020;21(6):2437-2445.
52. Murata M, Nakai Y, Kawazu K, *et al.* Loliolide, a carotenoid metabolite, is a potential endogenous inducer of herbivore resistance. Plant Physiol 2019;179(4):1822-1833.
53. Shah Z, Badshah S, Iqbal A, *et al.* GC-MS based metabolomics and lipidiomics analyses of selected freshwater green macroalgae. Res Sq 2022;0:1-25.
54. Rienth M, Vigneron N, Darriet P, *et al.* Grape berry secondary metabolites and their modulation by abiotic factors in a climate change scenario - a review. Front Plant Sci 2021;12:643258.
55. Salimi YK, Ode L, Wathoni Z, *et al.* Screening of Secondary Metabolite Compounds of Gorontalo Traditional Medicinal Plants Using the In Silico Method as a Candidate for SARS-CoV-2 Antiviral. JKSA 2022;25(10):382-393.
56. Chaniad P, Phuwajaroanpong A, Techarang T, *et al.* Antiplasmodial activity and cytotoxicity of plant extracts from the Asteraceae and Rubiaceae families. Heliyon 2022;8(1):e08848.
57. Cheng Q, Li F, Yan X, *et al.* Phytochemical and pharmacological studies on the genus Arcangelisia: A mini review. Arab J Chem 2021;14(10):103346.

58. Jing W, Xiaolan C, Yu C, *et al.* Pharmacological effects and mechanisms of tannic acid. Biomed Pharmacother 2022;154:113561.
59. Wang XQ, Wang W, Peng M, *et al.* Free radicals for cancer theranostics. Biomaterials 2021;266:120474.
60. Oladimeji BM, Adebo OA. Dataset of metabolites extracted from African walnut (*Tetracarpidium conophorum*) using two different solvents. Data Brief 2023;47:108930.
61. Rebryk A, Gallampois C, Haglund P. A time-trend guided non-target screening study of organic contaminants in Baltic Sea harbor porpoise (1988–2019), guillemot (1986–2019), and white-tailed sea eagle (1965–2017) using gas chromatography–high-resolution mass spectrometry. Sci Total Environ 2022;829:154620.
62. Pan G, Deshpande M, Pang H, *et al.* 4-Hydroxy-2-nonenal attenuates 8-oxoguanine DNA glycosylase 1 activity. J Cell Biochem 2020;121(12):4887-4897.
63. Api AM, Belsito D, Botelho D, *et al.* RIFM fragrance ingredient safety assessment, 2,3-dethylpyrazine, CAS registry number 15707-24-1. Food Chem Toxicol 2023;176 Suppl 1:113710.
64. Song HY, Yang JY, Suh JW, *et al.* Acaricidal activities of apiol and its derivatives from petroselinum sativum seeds against dermatophagoides pteronyssinus, dermatophagoides farinae, and tyrophagus putrescentiae. J Agric Food Chem 2011;59(14):7759-7764.
65. Rinaldi de Alvarenga JF, Lei Preti C, Santos Martins L, *et al.* Identification of D-limonene metabolites by LC-HRMS: An exploratory metabolic switching approach in a mouse model of diet-induced obesity. Metabolites 2022;12(12):1246.
66. Šunić L, Ilić ZS, Stanojević L, *et al.* Comparison of the essential oil content, constituents and antioxidant activity from different plant parts during development stages of wild fennel (*Foeniculum vulgare* Mill.). Horticulturae 2023;9(3):364.
67. Nowak I, Issayeva A, Dąbrowska M, *et al.* Possibilities of using medicinal plant extracts and salt-containing raw materials from the Aral region for cosmetic purposes. Molecules 2022;27(16):5122.
68. Sonigra P, Meena M. Metabolic profile, bioactivities, and variations in the chemical constituents of essential oils of the *Ferula* genus (Apiaceae). Front Pharmacol 2021;11:608649.
69. Xiao Y, Huang Y, Chen Y, *et al.* Discrimination and characterization of the volatile profiles of five Fu brick teas from different manufacturing regions by using HS–SPME/GC–MS and HS–GC–IMS. Curr Res Food Sci 2022;5:1788-1807.
70. Geddo F, Antoniotti S, Querio G, *et al.* Plant-derived trans-β-caryophyllene boosts glucose metabolism and atp synthesis in skeletal muscle cells through cannabinoid type 2 receptor stimulation. Nutrients 2021;13(3):916.
71. Salvatore MM, Alves A, Andolfi A. Secondary metabolites produced by *Neofusicoccum* species associated with plants: A review. Agric Switz 2021;11(2):149.
72. Zhao F, Wang P, Lucardi RD, *et al.* Natural sources and bioactivities of 2,4-di-tert-butylphenol and its analogs. Toxins Basel 2020;12(1):35.
73. Anastassiadou M, Bellisai G, Bernasconi G, *et al.* Review of the existing maximum residue levels for 1,4-dimethylnaphthalene according to Article 12 of Regulation (EC) No 396/2005. EFSA J 2021;19(5):6597.
74. Iwueke AV, Ejekwumadu NJ, Chukwu EC, *et al.* Nutritional composition and GC-MS phytochemical analysis of *Thaumatococcus daniellii* leaves. Eur J Nutr Food Saf 2020;12(8):81-86.
75. Paparella A, Shaltiel-harpaza L, Ibdah M. β-Ionone: Its occurrence and biological function and metabolic engineering. Plants Basel 2021;10(4):754.
76. Das M, Prakash S, Nayak C, *et al.* Dihydroactinidiolide, a natural product against Aβ 25-35 induced toxicity in Neuro2a cells: Synthesis, in silico and in vitro studies. Bioorganic Chem 2018;81:340-349.
77. Priyanto JA, Prastya ME, Primahana G, *et al. Paederia foetida* Linn leaves-derived extract showed antioxidant and cytotoxic properties against breast carcinoma cell. HAYATI J Biosci 2023;30(2):271-280.
78. Lee JW, Ji SH, Kim GS, *et al.* Global profiling of various metabolites in platycodon grandiflorum by UPLC-QTOF/MS. Int J Mol Sci 2015;16(11):26786-26796.
79. Yang Q, Zhu Y, Peng W, *et al.* A new lycopodine-type alkaloid from *Lycopodium japonicum*. Nat Prod Res 2016;30(19):2220-2224.
80. Grazzia N, Boaventura S, Garcia VL, *et al.* Dihydroartemisinin, an active metabolite of artemisinin, interferes with *Leishmania braziliensis* mitochondrial bioenergetics and survival. Parasitol Res 2021;120(2):705-713.
81. Purwaningsih I, Maksum IP, Sumiarsa D, *et al.* A review of *Fibraurea tinctoria* and its component, berberine, as an antidiabetic and antioxidant. Molecules 2023;28(3):1294.
82. Collins DJ, Pilotti CA, Wallis AFA. Triterpene acids from some Papua New Guinea *Terminalia* species. Phytochemistry 1992;31(3):881-884.
83. Zhang L, Wang J, Li T, *et al.* Determination of the chemical components and phospholipids of velvet antler using UPLC/QTOF-MS coupled with UNIFI software. Exp Ther Med 2019;17(5):3789-3799.

84. Morrow NM, Burke AC, Samsoondar JP, *et al.* The citrus flavonoid nobiletin confers protection from metabolic dysregulation in high-fat-fed mice independent of AMPK. J Lipid Res 2020;61(3):387-402.
85. Gorzalczany S, Marrassini C, Miño J, *et al.* Antinociceptive activity of ethanolic extract and isolated compounds of *Urtica circularis*. J Ethnopharmacol 2011;134(3):733-738.
86. Sun LR, Qing C, Zhang YL, *et al.* Cimicifoetisides A and B, two cytotoxic cycloartane triterpenoid glycosides from the rhizomes of *Cimicifuga foetida*, inhibit proliferation of cancer cells. Beilstein J Org Chem 2007;3:3.
87. Cao Q, Jiang Y, Cui SY, *et al.* Tenuifolin, a saponin derived from Radix Polygalae, exhibits sleep-enhancing effects in mice. Phytomedicine 2016;23(14):1797-1805.
88. Hagihara M, Endo M, Hata K, *et al.* Neogenin, a receptor for bone morphogenetic proteins. J Biol Chem 2011;286(7):5157-5165.
89. Chen JY, Li PL, Tang XL, *et al.* Cycloartane triterpenoids and their glycosides from the rhizomes of *Cimicifuga foetida*. J Nat Prod 2014;77(9):1997-2005.
90. Liu Y, Schuppe AW, Zhao Y, *et al.* Synthesis of (-)-melazolide B, a degraded limonoid, from a natural terpene precursor. Tetrahedron Chem 2022;1:100011.
91. Wang D, Dong X, Nie Y, *et al.* A review on medical plants of genus *Siegesbeckia*: Phytochemical and pharmacological studies. Rec Nat Prod 2022;16(6):515-537.
92. Tarasov A, Giuliani N, Dobrydnev A, *et al.* 1,1,6-Trimethyl-1,2-dihydronaphthalene (TDN) sensory thresholds in riesling wine. Foods 2020;9(5):606.
93. Elmasri WA, Hegazy MEF, Aziz M, *et al.* Biofilm blocking sesquiterpenes from *Teucrium polium*. Phytochemistry 2014;103:107-113.
94. Pirvu L, Stefaniu A, Neagu G, *et al.* Studies on *Anemone nemorosa* L. extracts; polyphenols profile, antioxidant activity, and effects on Caco-2 cells by in vitro and in silico studies. Open Chem 2022;20(1):299-312.
95. Jo A, Yoo HJ, Lee M. Robustaflavone isolated from *Nandina domestica* using bioactivity-guided fractionation downregulates inflammatory mediators. Molecules 2019;24(9):1789.
96. Feng H, Jiang Y, Cao H, *et al.* Chemical characteristics of the sesquiterpenes and diterpenes from Lauraceae family and their multifaceted health benefits: A review. Heliyon 2022;8(12):e12013.
97. Zhang ZJ, He J, Li Y, *et al.* Three new sesquiterpenes from *Laggera pterodonta*. Helv Chim Acta 2013;96(4):732-737.
98. Liang Y, Zhao W, Wang C, *et al.* A comprehensive screening and identification of genistin metabolites in rats based on multiple metabolite templates combined with UHPLC-HRMS analysis. Molecules 2018;23(8):1862.
99. Heinonen SM, Hoikkala A, Wähälä K, *et al.* Metabolism of the soy isoflavones daidzein, genistein and glycitein in human subjects. Identification of new metabolites having an intact isoflavonoid skeleton. J Steroid Biochem Mol Biol 2003;87(4-5):285-299.
100. Chen F, Li HL, Tan YF, *et al.* Different accumulation profiles of multiple components between pericarp and seed of alpinia oxyphylla capsular fruit as determined by UFLC-MS/MS. Molecules 2014;19(4):4510-4523.
101. Pratama MRF, Suratno S, Mulyani EVI. Antibacterial activity of akar kuning (*Arcangelisia flava*) secondary metabolites: Molecular docking approach. Asian J Pharm Clin Res 2018;11(11):447-451.
102. Kiefer JR, Pawiitz JL, Moreland KT, *et al.* Structural insights into the stereochemistry of the cyclooxygenase reaction. Nature 2000;405(6782):97-101.
103. Soberman RJ, Christmas P. The organization and consequences of eicosanoid signaling. J Clin Invest 2003;111(8):1107-1113.
104. Swiatek P, Glomb T, Dobosz A, *et al.* Biological evaluation and molecular docking studies of novel 1,3,4-oxadiazole derivatives of 4,6-dimethyl-2-sulfanylpyridine-3-carboxamide. Int J Mol Sci 2022;23(1):549.
105. Glomb T, Wiatrak B, Gębczak K, *et al.* New 1,3,4-oxadiazole derivatives of pyridothiazine- 1,1-dioxide with anti-inflammatory activity. Int J Mol Sci 2020;21(23):9122.
106. Xu S, Hermanson DJ, Banerjee S, *et al.* Oxicams bind in a novel mode to the cyclooxygenase active site via a two-water-mediated H-bonding network. J Biol Chem 2014;289(10):6799-6808.
107. Megantara S, Agung Yodha MW, Sahidin I, *et al.* Pharmacophore screening and molecular docking of phytoconstituents in *Polygonum sagittatum* for cyclooxygenase-2 inhibitors discovery. Asian J Pharm Clin Res 2018;11(1):83-88.
108. Singh S, Bani Baker Q, Singh DB. Molecular docking and molecular dynamics simulation. In: Singh DB, Pathak RK, editors. Bioinformatics: Methods and applications. London: Academic Press; 2021.
109. El-Feky AM, El-Rashedy AA. Sterols and flavonoids in strawberry calyx with free radical scavenging, anti-inflammatory, and molecular dynamic study. Beni-Suef Univ J Basic Appl Sci 2023;12:108.